

Gravitational Waves from Walking Technicolor

Kohtaroh Miura,^{1,2,*} Hiroshi Ohki,^{3,†} Saeko Otani,^{3,‡} and Koichi Yamawaki^{2,§}

¹*Helmholtz-Institut Mainz, Johannes Gutenberg-Universität Mainz, D-55099 Mainz, Germany*

²*Kobayashi-Maskawa Institute for the Origin of Particles and the Universe,
Nagoya University, Nagoya 464-8602, Japan*

³*Department of Physics, Nara Women's University, Nara 630-8506, Japan*

We study gravitational waves from the first-order electroweak phase transition in the $SU(N_c)$ gauge theory with $N_f/N_c \gg 1$ (“large N_f QCD”) as a candidate for the walking technicolor, which is modeled by the $U(N_f) \times U(N_f)$ linear sigma model with classical scale symmetry (without mass term), particularly for $N_f = 8$ (“one-family model”). This model exhibits spontaneous breaking of the scale symmetry as well as the $U(N_f) \times U(N_f)$ radiatively through the Coleman-Weinberg mechanism à la Gildener-Weinberg, thus giving rise to a light pseudo dilaton (techni-dilaton) to be identified with the 125 GeV Higgs. This model possess a strong first-order electroweak phase transition due to the resultant Coleman-Weinberg type potential. We estimate the bubble nucleation that exhibits an ultra supercooling and then the signal for a stochastic gravitational wave produced via the strong first-order electroweak phase transition. We show that the amplitude can be reached to the expected sensitivities of the LISA.

I. INTRODUCTION

The origin of mass is one of the most important issues in particle physics. In the standard model (SM), the parameters of the Higgs boson mass and the electroweak symmetry breaking scale are all free parameters, so that the dynamical origin of mass is a challenging issue. One attractive model beyond the standard model is the walking technicolor, in which the electroweak symmetry is dynamically broken due to approximately scale-invariant strong gauge dynamics (i.e. ladder Schwinger-Dyson (SD) equation) with large anomalous dimension $\gamma_m \simeq 1$ [1, 2],^{#1} in contrast to the original technicolor [6, 7] as a simple scale-up of the QCD. Due to the spontaneously broken approximate scale invariance, the walking technicolor model predicts [1, 2] a pseudo-dilaton (“technidilaton”), a pseudo Nambu-Goldstone (NG) boson of the spontaneously broken approximate scale symmetry, which could be identified with the Higgs boson with mass 125 GeV (see [8] and references cited therein).

The most popular candidate dynamics for the walking technicolor is the “large N_f QCD”, the $SU(N_c)$ gauge theory with $N_f (\gg N_c)$ fermions in the fundamental representation, where the theory has the Caswell-Banks-Zaks (CBZ) infrared fixed point [9, 10] for some larger N_f (conformal window), thereby becoming scale invariant at the fixed point. It is then expected that a walking gauge theory is realized for N_f just below the conformal window, the phase boundary of which is roughly estimated to be $N_f/N_c \lesssim 4$ [11], based on the two-loop beta function combined with the ladder SD equation, which is justified at least qualitatively for the large N_f QCD in the “anti-Veneziano limit” $N_c \rightarrow \infty$ with $N_f/N_c = \text{fixed} \gg 1$ [8] (cf. Veneziano limit with $N_f/N_c \ll 1$). In the walking phase the (approximate) scale symmetry as well as the chiral symmetry is spontaneously broken, thus we expect existence of the flavor-singlet scalar meson, σ , as light enough to be identified with the pseudo dilaton.

*kohmiura@uni-mainz.de

†hohki@asuka.phys.nara-wu.ac.jp

‡otani@asuka.phys.nara-wu.ac.jp

§yamawaki@kmi.nagoya-u.ac.jp

^{#1} The walking technicolor was subsequently studied [3, 4] without notion of the scale invariance/dilaton and anomalous dimension, along the line of the earlier numerical study [5].

Recently the lattice simulations of large N_f QCD for $N_c = 3$ have been widely studied to find such a walking behavior. Among others it was found [12–14] that $N_f = 8, N_c = 3$ QCD has a walking behavior with signals of the spontaneously broken phase and the approximate scale symmetry (non-universal hyperscaling with $\gamma_m \simeq 1$). More interestingly, a light σ meson was in fact discovered in the $N_f = 8, N_c = 3$ QCD on the lattice [15–18]. While the results have been obtained in the presence of the non-zero fermion mass m_f , in contrast to the walking technicolor model defined at vanishing fermion mass, it encourages us to consider a possibility of the composite dilaton (=Higgs/technidilaton) as a light bound state of the flavor singlet scalar in the large N_f QCD.

The $N_f = 8$ QCD is also attractive from the point of view of the model building, since the 8 flavors of the fermion in this model can be assigned as the four electroweak doublets in the one-family technicolor model, which is a model naturally fit in the extended technicolor (ETC) model to explain the dynamical origin of all the masses including the quarks and leptons [19].

Another interesting feature in large N_f QCD is its thermodynamic properties. As argued by Pisarski and Wilczek [20], in the QCD for $N_f > 2$ the finite temperature phase transition should be of first-order. If it is the case, the large N_f QCD as a walking technicolor should be quite attractive from the view of physics beyond the SM, since the SM which, having the same symmetry structure as that of the $N_f = 2$ QCD, is believed to have the strength of the electroweak phase transition not strong enough. Actually it is a key condition to explain the universe’s matter dominance in the electroweak baryogenesis scenario. Thus a possibility for the strong first-order electroweak phase transition should be a key ingredient for the walking technicolor as a large N_f QCD to account for the origin of the universe’s matter dominance.

In this paper we examine if the transition of the finite temperature electroweak phase transition in the early universe is of the first-order in the large N_f QCD with $N_f = 8$ as a walking technicolor model. If it is the case, the gravitational wave signal will be a good probe to the first-order phase transition in the early universe [21].

In fact such a gravitational wave can be detected by the future satellite observations such as the LISA [22, 23] and DECIGO [24, 25] whose sensitivity will reach the magnitude of the expected electroweak phase transition. Based on these recent developments on the gravitational wave signals, we here examine the electroweak bubble nucleation in thermal phase transition. Since fully nonperturbative analyses of the large N_f QCD such as the lattice studies are presently not available for this purpose, we need to adopt some effective theory approach.

An effective theory of the large N_f QCD as a candidate for the walking technicolor has been given by the (approximately) scale-invariant nonlinear sigma model, including the non-zero fermion mass effects to be compared with the lattice data [26].^{#2} In the chiral limit $m_f = 0$ which is the case for the walking technicolor, this is a version of the nonlinear sigma model consisting of $N_f^2 - 1$ composite pseudo NG bosons living on the manifold $G/H = SU(N_f)_L \times SU(N_f)_R / SU(N_f)_V$ plus a composite flavor-singlet scalar, σ , or the dilaton $\phi = \ln(\sigma/\langle\sigma\rangle)$ ($\langle\phi\rangle = 0$) with the decay constant $F_\phi = \langle\sigma\rangle$, to realize the scale symmetry nonlinearly. In addition it possesses a small explicit breaking of the scale symmetry in the form of the Coleman-Weinberg (CW) type log potential consisting only of the dilaton (now becoming a pseudo dilaton (technidilaton) identified with the 125 GeV Higgs), which reproduces the trace anomaly in the underlying large N_f QCD (see [8] and the references therein). The appearance of the CW type dilaton potential is already a good signal of the first-order phase transition.

In this work, however, we adopt a more conventional systematic approach towards this problem, based on the perturbation for the linear sigma model as an effective theory of the large N_f QCD with $N_f = 8$. (For a different approach based on the holographic walking technicolor, see [33]). The model has the same symmetry as the underlying large N_f QCD, namely the chiral $U(N_f)_L \times U(N_f)_R$ symmetry together with the scale symmetry (without scalar mass term) at classical level. These symmetries are spontaneously broken as well as explicitly broken by the chiral anomaly and the trace anomaly at the quantum level in the underlying theory. Also in the linear sigma model it is possible to break the scale and the chiral symmetry spontaneously at quantum level by the conventional CW mechanism now consistently formulated in the perturbation at one loop in a large N_f version proposed by Gildener and Weinberg (GW) [34, 35]. In the GW model, there exists a scale-invariant flat direction along the flavor-singlet field σ in the classical potential at some renormalization scale, say μ_{GW} , which makes the perturbation fully consistent. The flat direction actually is lifted by quantum corrections at one loop, so that the spontaneous chiral and scale symmetry breaking occurs in this direction, with the scale symmetry also broken explicitly as the trace anomaly due to the very loop effects.

One striking feature in the GW mechanism is that the flavor-singlet scalar $\sigma = e^{\phi/\langle\sigma\rangle}$ becomes a light scalar (what they called “scalón”) after the symmetry breaking, which is nothing but a pseudo dilaton ϕ , the pseudo NG boson of the spontaneously broken scale symmetry (also explicitly broken by the trace anomaly). The CW potential

^{#2} For subsequent studies on the candidate effective theory for a light scalar boson in the large N_f QCD on the lattice, see Refs. [27–30] via nonlinear realization and [31, 32] on the linear sigma model.

consists only of this pseudo dilaton. We will in fact see that the CW potential obtained in the perturbation at the effective theory level is consistent with the aforementioned scale-invariant nonlinear sigma model with the CW type dilaton potential [26] based on the nonperturbative method, the ladder approximation/anti-Veneziano limit, in the underlying large N_f QCD. Thus the free parameters in our model may be estimated, the quartic couplings < 1 and $\langle \sigma \rangle = F_\phi \simeq 5 v_{\text{EW}} \simeq 1.25 \text{ TeV}$ ($\gg v_{\text{EW}} = 246 \text{ GeV}$), under matching with those of the CW type dilaton potential in the $N_f = 8$ walking technicolor [26], which were well fit to the LHC data for the 125 GeV Higgs.

With the parameters so determined as bench mark values in the linear sigma model as an effective theory of the large N_f QCD with $N_f = 8$, we find that in the corresponding walking technicolor we naturally obtain a very strong first-order phase transition, thanks to the nature of the GW formulation of the CW, in sharp contrast to the SM. We further find that this phase transition yields an ultra supercooling, from which a significant amount of the gravitational wave signals can be produced to be tested in future experiments such as LISA and DECIGO.

It should be noted here that in our model it is not necessary to introduce an elementary Higgs scalar particle in sharp contrast to the other composite Higgs boson scenarios such as dark QCD. Recent studies of the gravitational wave signals from the first-order phase transition in composite Higgs models can be found in e.g. [36–40]. In most of models, the thermal phase transition can occur in a two (or more)-dimensional field space, which makes the bubble nucleation analysis more complicated. In our model, however we provide a simple mechanism that can exhibit the electroweak symmetry breaking, together with a non-zero Higgs (pseudo dilaton) vev.

The paper is organized as follow. In sec. II, the setup of our model will be shown, where the dilaton potential for the singlet scalar can be obtained with a quantum effect. It is explained how our model is dedicated to be the effective model of the walking technicolor model. In Sec. III, we study the finite temperature effect on the dilaton potential for which we see a strong first-order phase transition. In Sec. IV, we investigate the bubble nucleation dynamics and the gravitational wave spectra in this model. We also provides some discussion on the flavor non-singlet scalar mass and show the corresponding phase diagram. Sec. V is devoted to a summary and concluding remarks. Some details of the formulas for the external mass effects and the gravitational wave spectra are provided in Appendix A and B, respectively.

II. SCALE INVARIANT LINEAR SIGMA MODEL AND DILATON EFFECTIVE POTENTIAL

We consider a linear sigma model having $U(N_f)_L \times U(N_f)_R$ chiral symmetry as an effective theory of the underlying large N_f QCD. A matrix of $N_f \times N_f$ denoted by M_{ab} is an effective scalar field, which transforms under chiral symmetry of $U(N_f)_L \times U(N_f)_R$ as

$$M \rightarrow g_L M g_R^\dagger, \quad g_L, g_R \in U(N_f). \quad (1)$$

A basis of $N_f \times N_f$ Hermitian matrices $T^a (a = 0, \dots, N_f^2 - 1)$ is used to become flavor diagonal, which satisfy the following conditions as

$$\text{Tr}[T^a, T^b] = \delta^{ab}/2. \quad (2)$$

Here $T^0 = \frac{1}{\sqrt{2N_f}} \mathbb{1}_{N_f \times N_f}$ is the non traceless matrix. The matrix field M can be decomposed as

$$M = \sum_{a=0}^{N_f^2-1} (s^a + ip^a) T^a, \quad (3)$$

where s^a and p^a are the N_f^2 scalars (0^{++}) and N_f^2 pseudoscalars (0^{-+}), respectively.

We consider the following renormalizable effective Lagrangian with classically scale invariance,

$$\mathcal{L} = \text{Tr}[\partial_\mu M^\dagger \partial^\mu M] - V_0(M), \quad (4)$$

where V_0 is the tree level potential given by $U(N_f)_L \times U(N_f)_R$ invariant forms,

$$V_0 = f_1 (\text{Tr}[M^\dagger M])^2 + f_2 \text{Tr}[(M^\dagger M)^2]. \quad (5)$$

Since we assume that the chiral symmetry breaks down to the diagonal subgroup $SU(N_f)_L$, it is natural to restrict the vev to its hypersphere,

$$\langle M \rangle = T^0 \langle s^0 \rangle = \frac{1}{\sqrt{2N_f}} \mathbb{1} \cdot \langle s^0 \rangle. \quad (6)$$

Following Ref. [34] let us briefly review the potential analysis at one loop level (see also [35] for the $U(N_f)_L \times U(N_f)_R$ notation). If we have

$$f_1 = -f_2/N_f, \quad f_2 > 0, \quad (7)$$

there is a stationary point of the potential with $V_0 = 0$ for non-zero values for M . In particular, if we restrict the field value of M to its radial component, the potential has a flat direction along the radial component which can always be chosen to be s^0 by the chiral rotation, with all the other field values set to zero.

The flat direction at tree level will be lifted by the quantum corrections, which generate a potential minimum for a non-zero value of s^0 . As it was shown in Ref. [34], with suitable renormalization conditions it is possible to take the value of the couplings such that $f_1 = -\frac{f_2}{N_f}$ at a scale μ_{GW} . Then the one loop potential V_1 can be expressed as

$$V_1(M) = \frac{1}{64\pi^2} \sum_{a=0}^{N_f^2-1} \left(m_{s^a}^4(M) \left(\ln \frac{m_{s^a}^2(M)}{\mu_{GW}^2} - \frac{3}{2} \right) + m_{p^a}^4(M) \left(\ln \frac{m_{p^a}^2(M)}{\mu_{GW}^2} - \frac{3}{2} \right) \right), \quad (8)$$

where $m_{s^a}^2$ and $m_{p^a}^2$ are the mass functions for scalars and pseudoscalars:

$$m_{s^a}^2 = \frac{\partial^2 V_0(M)}{\partial (s^a)^2}, \quad m_{p^a}^2 = \frac{\partial^2 V_0(M)}{\partial (p^a)^2}. \quad (9)$$

By setting $p^a = 0$ and $s^i = 0$, we define the s^0 -dependent mass functions, which are given as

$$\begin{aligned} m_{s^0}^2(s^0) &= 0, & m_{s^i}^2(s^0) &= \left(f_1 + f_2 \frac{3}{N_f} \right) (s^0)^2 = \frac{2f_2}{N_f} (s^0)^2, \\ m_{p^a}^2(s^0) &= 0, & m_{p^i}^2(s^0) &= 0. \end{aligned} \quad (10)$$

As mentioned above, if the GW condition is satisfied, the tree level potential is flat for the direction s^0 , and the effective potential for s^0 is given

$$\begin{aligned} V_{\text{eff}}(s^0) &= V_{\text{eff}}(M)|_{M \rightarrow T^0 s^0} = (V_0(M) + V_1(M))|_{M \rightarrow T^0 s^0} \\ &= \frac{N_f^2 - 1}{64\pi^2} m_{s^i}^4(s^0) \left(\ln \frac{m_{s^i}^2(s^0)}{\mu_{GW}^2} - \frac{3}{2} \right), \end{aligned} \quad (11)$$

The stationary condition for s^0 is obtained from the derivative of $V_{\text{eff}}(s^0)$,

$$\begin{aligned} 0 &= \frac{\partial V_{\text{eff}}(s^0)}{\partial s^0} \Big|_{s^0 \rightarrow \langle s^0 \rangle} \\ &= \frac{f_2^2}{4\pi^2} \frac{N_f^2 - 1}{N_f^2} \langle s^0 \rangle^3 \left(\ln \frac{m_{s^i}^2(\langle s^0 \rangle)}{\mu_{GW}^2} - 1 \right). \end{aligned} \quad (12)$$

Thus a nonzero vev for s^0 is determined,

$$\ln \frac{m_{s^i}^2(\langle s^0 \rangle)}{\mu_{GW}^2} = 1 \quad \Rightarrow \quad \langle s^0 \rangle = \sqrt{\frac{e N_f}{2 f_2}} \mu_{GW}. \quad (13)$$

Due to no tree level contribution in the effective potential the stationary condition is only determined from the loop correction, where the logarithmic term of a perturbative correction given by $(\ln(m_{s^i}^2(\langle M \rangle)/\mu_{GW}^2) - \frac{3}{2})$ does not depend on the inverse power of f_2 in contrast to a general CW potential, and stays small ($\mathcal{O}(1)$). Therefore the perturbation analysis should work.

Thus we see that for the flat direction along the radial component s^0 , the vacuum degeneracy can be lifted by the quantum correction, which give rise to the mass of s^0 , which reads

$$m_{s^0}^2 = \frac{\partial^2 V_{\text{eff}}(M)}{\partial (s^0)^2} \Big|_{M=\langle M \rangle=T^0 \langle s^0 \rangle} = \frac{f_2^2}{2\pi^2} \frac{N_f^2 - 1}{N_f^2} \langle s^0 \rangle^2 = \frac{e f_2}{4\pi^2} \left(\frac{N_f^2 - 1}{N_f} \right) \mu_{GW}^2. \quad (14)$$

Among the flavor non-singlet scalars s^i 's the iso non-singlet scalars^{#3} have a common positive definite mass, which reads from Eq.(10) and Eq.(13):

$$m_{s^i}^2 = \left. \frac{\partial^2 V_{\text{eff}}(M)}{\partial (s^i)^2} \right|_{M=\langle M \rangle} = m_{s^i}^2(\langle s^0 \rangle) = e\mu_{GW}^2. \quad (15)$$

From Eq. (15) and Eq.(14) we have

$$\frac{m_{s^0}^2}{m_{s^i}^2} = \frac{f_2 N_f}{4\pi^2} \left(\frac{N_f^2 - 1}{N_f^2} \right) \quad \left(\ll 1 \quad \text{for} \quad \frac{f_2 N_f}{4\pi^2} \ll 1 \right), \quad (16)$$

where the 't Hooft coupling $f_2 N_f$ is fixed in the anti-Veneziano limit $N_c \rightarrow \infty$ with $N_f/N_c = \text{fixed} (> 1)$ of the underlying large N_f QCD.

As for the N_f^2 pseudoscalars, p^a 's, they still remain massless due to the other flat directions, which correspond to the pion fields (π^a), the massless NG bosons of the chiral symmetry breaking $U(N_f)_L \times U(N_f)_R / U(N_f)_V$.

These massless NG bosons can have mass as follows: In the underlying large N_f QCD, the axial $U(1)_A$ anomaly for the N_f fermions should be responsible for the mass of flavor-singlet " η' ", which could be even much heavier than in the ordinary QCD particularly in the anti-Veneziano limit $N_c \rightarrow \infty$ with $N_f/N_c \gg 1$ (the limit corresponding to the walking technicolor) [8], in good agreement with the preliminary lattice results [41]. Under this circumstance we simply assume this η' as super heavy to be decoupled in the linear sigma model treatment for $N_f = 8$ in the present paper. ^{#4} The rest of $N_f^2 - 1$ NG bosons in the $N_f = 8$ one-family technicolor model are no longer massless; The chiral symmetry $SU(8)_L \times SU(8)_R$ are explicitly broken down to $SU(2)_L \times U(1)_Y$ through the SM gauge interactions (QCD and electroweak) and the ETC gauge interactions, so that 60 NG bosons acquire the mass (becoming pseudo NG bosons), leaving us with only three of them which are of course absorbed into W/Z bosons via the standard Higgs mechanism. Masses of all these 60 pseudo NG bosons are enhanced in the walking theory by the large anomalous dimension $\gamma_m \simeq 1$. In this paper, instead of explicitly formulating these effects, we shall employ a handy way by simply introducing ad hoc mass breaking at tree level into the linear sigma model in subsection IIB.

A. Equivalence to the dilaton potential in the walking technicolor

We discuss the possibility that this light scalar s^0 in the above frame may be regarded as the pseudo dilaton, the pseudo NG boson associated with the approximate scale invariance, which is nothing but a technidilaton in the context of the walking technicolor.

In fact we notice that the scalar potential in Eq.(11) is equivalent to the CW-like dilaton potential for the walking technicolor, Eq. (3) (with the spurion set to be $S = 1$) in Ref. [26],

$$\mathcal{L}_{(2)\text{hard}} = -\frac{m_\phi^2 F_\phi^2}{4} \chi^4 \left(\ln \chi - \frac{1}{4} \right) = -\frac{m_\phi^2}{4F_\phi^2} \sigma^4 \left(\ln \frac{\sigma}{F_\phi} - \frac{1}{4} \right), \quad (F_\phi \equiv \langle \sigma \rangle) \quad (17)$$

where $\sigma(x) \equiv F_\phi \cdot \chi(x)$ with $\chi(x) \equiv e^{\phi(x)/F_\phi}$ is a chiral singlet field with the canonical dimension 1 under the scale transformation and is related to the dilaton field $\phi(x)$ s.t. $\langle \phi(x) \rangle = 0$ ($\langle \chi(x) \rangle = 1$),^{#5} with the dilaton decay constant, $F_\phi (= \langle \sigma \rangle)$, and $m_\phi (\simeq 125 \text{ GeV})$ is the mass of the (pseudo) dilaton ϕ to be identified with the 125 GeV Higgs. It indeed reproduces the PCDC relation $m_\phi^2 F_\phi^2 = -F_\phi \langle 0 | \partial^\mu D_\mu | \phi \rangle = -d_\theta \langle \theta_\mu^\mu \rangle = -d_\theta \langle \delta_D \mathcal{L}_{(2)\text{hard}}^S \rangle$ with $d_\theta = 4$. The trace anomaly $\theta_\mu^\mu \neq 0$ measuring the explicit breaking of the scale symmetry comes from the spontaneous breaking of the chiral symmetry and the scale symmetry in the scale-invariant dynamics (ladder SD equation, à la anti-Veneziano limit) for the underlying large N_f QCD, which generates the spontaneous breaking mass scale actually provided by the cutoff regulator or the renormalization point. See [8] and references therein. ^{#6}

^{#3} As for the iso-singlet scalars, the mass function is not positive definite for $N \geq 3$ at one loop level. This problem can be avoided by adding a small explicit breaking mass term, and we will discuss phenomenological implication of such effect.

^{#4} The effect of $U(1)_A$ breaking effect in the linear sigma model at tree-level has been recently discussed [31] to understand the lightness of the singlet scalar on the lattice [41].

^{#5} The scale (dilatation) transformations for these fields are $\delta_D \sigma = (1 + x^\mu \partial_\mu) \sigma$, $\delta_D \chi = (1 + x^\mu \partial_\mu) \chi$, $\delta_D \phi = F_\phi + x^\mu \partial_\mu \phi$. Although χ is a dimensionless field, it transforms as that of dimension 1, while ϕ having dimension 1 transforms as the dimension 0, instead.

^{#6} The same effective potential was directly derived in the the "quenched QED₄" [42] up to trivial factors of N_c and N_f , resulting in the same PCDC relation.

Now for the present case of the linear sigma model we may write $\sigma^2 = 2\text{Tr}(M^\dagger M)$, with σ being the field in the ray (radial) direction in the tree potential as in the GW arguments and actually the same field as σ in Eq.(17) to be obviously chiral singlet having the canonical scale dimension 1. The trace expression can always be rotated into $2\text{Tr}(M^\dagger M) \rightarrow (s^0)^2$ by the chiral transformation into a particular frame $s^i, p^a \rightarrow 0$, so that $\sigma^2 = (s^0)^2$, namely we can identify σ with s^0 . Thus the two free parameters f_2 and $\langle s^0 \rangle$ (or, μ_{GW}) in our model are related to the dilaton mass $m_{s^0} = m_\phi \simeq 125$ GeV and its decay constant $F_\phi = \langle s^0 \rangle$ in the dilaton potential. The value of F_ϕ of a technidilaton as the 125 GeV Higgs, $m_\phi = 125$ GeV, is estimated [8] through the best fit to the LHC data for the 125 GeV Higgs as $F_\phi \simeq 1.25\text{TeV} \simeq 5 v_{\text{EW}}$ ($N_f = 8, N_c = 4$), which is also consistent with the ladder estimate for the trace anomaly $\langle \theta_\mu^\mu \rangle = 4\langle \theta_0^0 \rangle$ and v_{EW} in the large N_f QCD.

Comparing Eq.(17) with Eq.(11), we find the following identifications for $N_f = 8$ in the frame mentioned above:

$$\begin{aligned} s^0 &= \sigma = F_\phi \cdot e^{\phi/F_\phi}, & \langle s^0 \rangle &= \langle \sigma \rangle = F_\phi \simeq 5 \cdot v_{\text{EW}} \simeq 1.25 \text{ TeV}, \\ f_2^2 &= 2\pi^2 \frac{m_\phi^2}{F_\phi^2} \frac{N_f^2}{N_f^2 - 1} \simeq (0.45)^2 \ll 1, \end{aligned} \quad (18)$$

where the numerical values for F_ϕ and f_2 are for the best fit value to the LHC data for the 125 GeV Higgs mentioned above, and will be our bench mark value in the later discussions. Thus s^0 (more precisely the frame-independent radial field σ , the flavor singlet scalar) plays a role of the pseudo dilaton $\phi = \ln(\sigma/\langle \sigma \rangle)$ as originally referred to as ‘‘scalon’’ in Ref. [34]. Note that $F_\phi^2 \sim N_f N_c \sim N_f^2$ in the anti-Veneziano limit of the underlying large N_f QCD and hence $f_2 N_f = \text{fixed}$ in that limit. #7

Thus the same symmetry relation should hold in our potential. Our result indicates that the low energy effective theory of large N_f QCD can be approximately described by a linear sigma model having the scale invariance in the weak coupling regime $f_2 \simeq 0.45 (< 1)$ and $|f_1| = |-f_2/N_f| \simeq 0.056 \ll 1$, where the perturbative picture works at the composite level.

For the analyses on the electroweak phase transition and the gravitational wave signals, the perturbative analysis of thermal potential should be valid due to our bench mark values in Eq.(18), the large value of $F_\phi \simeq 1.25$ TeV and small $f_2 \simeq 0.45 < 1$. In addition, the radiative corrections to the effective potential from SM particles could be subdominant due to a large value of F_ϕ , so that we neglect them in the following analysis.

For discussing the electroweak phase transition, one might literally gauge the linear sigma model kinetic term in Eq.(4), with the electroweak W/Z bosons, in which case the W/Z boson mass scale would be given by $\langle s^0 \rangle = v_{\text{EW}} = 246$ GeV in apparent contradiction with our bench mark value $\langle s^0 \rangle = F_\phi \simeq 5 v_{\text{EW}}$ in Eq.(18). Note that Eq.(18) is based on the dilaton effective theory in Ref. [26], whose kinetic term is

$$\mathcal{L}_{(2)}^{(\text{inv})} = \frac{F_\phi^2}{2} (\partial_\mu \chi)^2 + \frac{F_\pi^2}{4} \chi^2 \text{Tr} [\partial_\mu U \partial^\mu U^\dagger], \quad U(x) \equiv \exp\left(\frac{2i\pi(x)}{F_\pi}\right), \quad \pi(x) \equiv \sum_{i=1}^{N_f^2-1} \pi^i(x) T^i. \quad (19)$$

where F_π is the decay constant of NG boson π to be absorbed into W/Z ($U(1)_A$ is explicitly broken by the axial anomaly in the underlying theory and is irrelevant to the W/Z mass anyway). This has the scale symmetry and chiral $SU(N_f)_L \times SU(N_f)_R$, both spontaneously broken, the same symmetry structure as that in the underlying large N_f QCD, where F_ϕ is in general different from $v_{\text{EW}} = \sqrt{N_f/2} \cdot F_\pi$ as shown in the ladder calculations à la anti-Veneziano limit. Indeed the kinetic term of $\pi(x)$ in Eq.(19) is normalized to be canonical for any value of F_π . #8 Actually, after the spontaneous symmetry breaking due to the log potential arising from quantum corrections, the linear sigma model kinetic term Eq.(4) may no longer be valid generically, particularly for the NG boson parts irrelevant to the potential, which is given by the second term in Eq.(19) as a most general effective theory of the underlying theory.

#7 For our bench mark value in Eq.(18), we would have $m_{s^0}^2/m_{s^i}^2 \simeq (0.3)^2$. Within the linear sigma model, this hierarchy can be further enlarged by introducing a large tree-level explicit mass term for p^a mocking up the explicit breaking due to the SM and ETC gauge interactions in the walking technicolor. See the next subsection.

#8 The linear sigma model kinetic term Eq.(4) corresponds to only a particular choice $F_\pi = F_\phi/\sqrt{N_f/2}$, where Eq.(19) rewritten in terms of $\tilde{M} = \sigma T^0 \cdot U = F_\phi \chi T^0 \cdot U$ takes precisely the same form as Eq.(4) for M . Alternatively, any complex matrix M can be written in the polar decomposition $M = H \cdot U$, where $H = \sum_{a=0}^{N_f^2-1} \tilde{s}^a T^a$ is the Hermitian matrix and U the unitary to be identified with the U in Eq.(19), then $\text{Tr}[\partial_\mu M^\dagger \partial^\mu M] = \text{Tr}[(\partial_\mu H)^2] + \text{Tr}[H^2 \partial_\mu U \partial^\mu U^\dagger]$. Although H contains massive $N_f^2 - 1$ flavor non-singlet scalar $\{s^i\} \sim \{\tilde{s}^i\}$ in addition to the light singlet scalar (pseudodilaton) $s^0 \sim \tilde{s}^0$, these massive components may be ignored in the decoupling limit as to set $H \sim s^0 T^0 = F_\phi \chi T^0$ at one loop (at higher loops in that limit, counter terms of the high dimensional operators will destroy such a simplest result, leading to the generic case Eq.(19)).

Thus the linear sigma model restriction $\langle s^0 \rangle = \sqrt{N_f/2} \cdot F_\pi = v_{\text{EW}}$ can be lifted in the generic effective theory of the large N_f QCD as the walking technicolor.

B. Soft chiral and scale symmetry breaking term

As mentioned earlier, the large N_f QCD in the walking regime would produce many massless NG bosons for the spontaneously broken large chiral symmetry $U(N_f)_L \times U(N_f)_R$, so does our linear sigma model with massless N_f^2 pseudoscalar p^a . In the underlying large N_f QCD, the flavor-singlet one “ η ” should acquire mass from the axial anomaly. When the theory is applied to the actual walking technicolor coupled to the SM gauge and ETC gauge interactions, these gauge interactions break explicitly the large chiral symmetry to give mass to other pseudoscalar NG bosons. In the case at hand $N_f = 8$, while the three among the rest 63 NG bosons should be eliminated by the Higgs mechanism of the gauged $SU(2)_L \times U(1)_Y$ symmetry, all the remaining 60 NG bosons should obtain mass from the SM and the ETC gauge interaction similarly to the $\pi^+ - \pi^0$ mass difference in the usual QCD. Although these couplings are weak to be perturbative, the large anomalous dimension $\gamma_m \simeq 1$ of the walking technicolor enhances all these masses to the TeV scale. For details see Ref. [8] and the references cited therein.

In the following analysis, instead of discussing these effects explicitly, here we consider an extension of the potential by simply adding some tree level mass term in the potential mocking up these explicit breakings. (For a study of the SM contributions to mass terms in the (non-conformal) linear sigma model, see Ref. [43]). Among various possibilities of the chiral symmetry breaking mass terms, we consider the following mass term ^{#9}

$$V_{\text{soft}} = \frac{(\Delta m_p)^2}{2} \sum_{a=0}^{N_f^2-1} (p^a)^2. \quad (20)$$

Then the tree-level potential is given by $V(M) = V_0(M) + V_{\text{soft}}(M)$. Comparing with Eq. (10), the s^0 -dependent mass functions for this model at tree level are modified as

$$\begin{aligned} m_{s^0}^2(s^0, \Delta m_p) &= 0, & m_{s^i}^2(s^0, \Delta m_p) &= \frac{2f_2}{N_f} (s^0)^2, \\ m_{p^a}^2(s^0, \Delta m_p) &= (\Delta m_p)^2. \end{aligned} \quad (21)$$

At one loop level, we immediately see that the stationary condition and the mass for s^0 are unchanged from the original potential since there is no s^0 dependence in the mass functions for the pseudoscalars (no $(s^0)^2(p^{(a)})^2$ couplings under the GW condition Eq.(7)) and the mass functions for the scalars are the same.^{#10} However, this potential also gives a mass to the non-singlet scalars through the quantum effect. Then the other mass spectra are modified as follows

$$\begin{aligned} m_{s^i}^2 &= e\mu_{\text{GW}}^2 + \frac{f_2}{32\pi^2} \left\{ 2N_f(\Delta m_p)^2 \left(\ln \left(\frac{(\Delta m_p)^2}{\mu_{\text{GW}}^2} \right) - 1 \right) + ef_2\mu_{\text{GW}}^2 \left(9 + \ln \left(\frac{(\Delta m_p)^2}{\mu_{\text{GW}}^2} \right) \right) \sum_{j=1}^{N_f^2-1} (d_{jji})^2 \right\} \\ m_{p^0}^2 &= (\Delta m_p)^2 + \frac{4f_2}{32\pi^2} \left(\frac{N_f^2 - 1}{N_f} \right) (\Delta m_p)^2 \left(\ln \left(\frac{(\Delta m_p)^2}{\mu_{\text{GW}}^2} \right) - 1 \right) \\ m_{p^i}^2 &= (\Delta m_p)^2 + \frac{f_2}{32\pi^2} \left(2N_f - \frac{4}{N_f} \right) (\Delta m_p)^2 \left(\ln \left(\frac{(\Delta m_p)^2}{\mu_{\text{GW}}^2} \right) - 1 \right), \end{aligned} \quad (22)$$

where d_{ijk} is the totally symmetric tensor

$$d_{ijk} = 2\text{Tr}[\{T^i, T^j\}T^k], \quad (23)$$

^{#9} While the above-mentioned SM and ETC gauge interactions leave the three NG bosons be exact massless to be absorbed into W/Z bosons, this mass term gives mass also to such NG bosons. However, for the purpose of the present paper to see the phase transition nature of the scalar sector relatively independent of W/Z mass generation, this would not be a serious problem.

^{#10} One might suspect that Eq.(20) would change in principle the mass of pseudo dilaton s^0 , since it breaks the scale symmetry explicitly. Although it in fact gives an additional contribution to the trace anomaly θ_μ^μ , the PCDC relation relevant to $\langle \theta_\mu^\mu \rangle$ is actually unchanged and so is the mass of s^0 as a pseudo dilaton, since the additional contributions to the relation are $\langle \Delta \theta_\mu^\mu \rangle \sim \langle (p^{(a)})^2 \rangle = 0$. This is indeed consistent with the explicit one loop calculations.

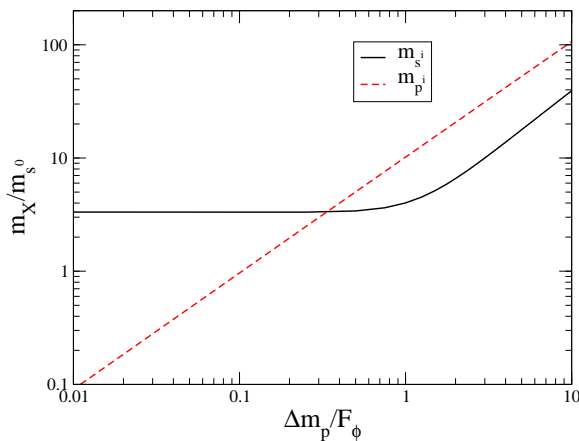


FIG. 1: Δm_p dependent mass ratio for $N_f = 8$ with $f_2 = 0.45$.

for the generators of $SU(N)$. As shown here, we see that the iso-singlet scalar mass can be negative in the vicinity of the zero mass $\Delta m_p \rightarrow 0$, since only the iso-singlet sector has a non-zero value for d_{ij} , and a log term which is proportional to d_{ij} becomes infinite in the limit $\Delta m_p \rightarrow 0$. Thus the mass function for the iso-singlet scalar becomes well defined if $\Delta m_p > \mu_{GW}$ for $N > 2$.

The resulting mass ratios obtained from the explicit mass terms are shown in Fig. 1. As shown here, a large mass hierarchy between the flavor singlet and non-singlet scalar masses is obtained without a tree-level scalar mass. While both the m_{p^i} and m_{s^i} have a linear dependence of the mass $(\Delta m_p)^2$, the coefficient for m_{s^i} is suppressed by a one-loop factor compared to Δm_p . Following again [26], let us assume that $s^0 \sim \sigma$ can be regarded as the pseudo dilaton, which corresponds to the Higgs boson with mass 125 GeV in SM, and the vev $\langle s^0 \rangle = \langle \sigma \rangle$ corresponds to the dilaton decay constant F_ϕ . As increasing Δm_p we see a large mass hierarchy between light pseudo dilaton and the others. Assuming $\Delta m_p \sim F_\phi \simeq 1.25$ TeV as a typical new physics scale beyond SM, we can obtain a mass of $\mathcal{O}(1)$ TeV for technihadrons.

We note that the additional potential term V_{soft} does not change the dilaton potential given in Eq. (17) at the one loop level. Thus the soft breaking mass parameter Δm_p provides a way of the decoupling limit for other meson fields: $m_{s^i, p^a} \rightarrow \infty$ simply by taking the limit $\Delta m_p \rightarrow \infty$. Even in the decoupling limit, the dilatonic nature of the flavor singlet scalar:

$$\left. \frac{\partial V_{\text{eff}}}{\partial s^0} \right|_{s^0=0} = 0, \quad \left. \frac{\partial^2 V_{\text{eff}}}{\partial (s^0)^2} \right|_{s^0=0} = 0, \quad (24)$$

remains intact.

From the result, we can expect that the first-order phase transition at finite temperature can naturally occur since a positive quadratic curvature at the origin can be easily generated through the thermal effect. We will examine the thermal phase transition for the dilaton potential in the next section. We also note that the perturbative correction of the logarithmic term is small in the effective potential for the radial direction $V_{\text{eff}}(s^0 \sim \sigma)$

$$V_{\text{eff}} = \frac{N_f^2 - 1}{64\pi^2} m_{s^i}^4(s^0, \Delta m_p) \left(\ln \frac{m_{s^i}^2(s^0, \Delta m_p)}{\mu_{GW}^2} - \frac{3}{2} \right) + C, \quad (25)$$

where C is a constant, so that the GW mechanism still works even if we have an additional parameter $(\Delta m_p)^2$.

III. FINITE TEMPERATURE POTENTIAL AND ELECTROWEAK PHASE TRANSITION

In this section we investigate the effective potential at finite temperature T [44, 45] and study the thermal phase transition of the chiral and scale symmetry. To evaluate the finite temperature effective potential, we use the one loop contribution of the thermal effect $V_{1,T}(s^0, T)$

$$V_{1,T}(s^0, T) = \frac{T^4}{2\pi^2} \sum_{a=0}^{N_f^2-1} \{ J_B(m_{s^a}^2(s^0, \Delta m_p)/T^2) + J_B(m_{p^a}^2(s^0, \Delta m_p)/T^2) \}, \quad (26)$$

where J_B is the bosonic thermal function

$$J_B(x) = \int_0^\infty t^2 \ln \left(1 - e^{-\sqrt{t^2+x}} \right) dt. \quad (27)$$

We directly evaluate Eq. (27) without expanding in its argument $m_{s^a}^2/T^2$. It is known that usual perturbative expansion valid at zero temperature will break down at high temperature where the higher loop contributions, in particular quadratic divergent loops (daisy diagrams), can not be neglected. We include the daisy diagrams which correspond to replace the mass functions in both zero and finite temperature effective potential (V_1 and $V_{1,T}$) with the effective T -dependent masses, $\mathcal{M}_{s^i}^2(s^0, \Delta m_p, T) = m_{s^i}^2(s^0, \Delta m_p) + \Pi(T)$, where,

$$\Pi(T) = \frac{T^2}{6} \left((N_f^2 + 1)f_1 + 2N_f f_2 \right) \Big|_{f_1 = -f_2/N_f}, \quad (28)$$

is the one-loop self-energy in the infrared limit in the leading order of the high temperature expansion $\propto T^2$ [46]. (For a pedagogical review, see [47]).

Using the mass functions given in Eq. (21), the total effective potential $V_{\text{eff}}(s^0, T)$ with the daisy diagrams is given as

$$V_{\text{eff}}(s^0, T) = \frac{N_f^2 - 1}{64\pi^2} \mathcal{M}_{s^i}^4(s^0, \Delta m_p, T) \left(\ln \frac{\mathcal{M}_{s^i}^2(s^0, \Delta m_p, T)}{\mu_{GW}^2} - \frac{3}{2} \right), \\ + \frac{T^4}{2\pi^2} (N_f^2 - 1) J_B(\mathcal{M}_{s^i}^2(s^0, \Delta m_p, T)/T^2) + C(T). \quad (29)$$

Here again $C(T)$ is a temperature dependent constant, which includes the pseudoscalar contributions. We note that $C(T)$ does not affect the phase transition dynamics, since the mass functions for pseudoscalars do not depend on s^0 . In the following, we use this effective potential to investigate the gravitational wave signal in the electroweak phase transition.

As will be shown later, the chiral phase transition described by our effective potential is of very strong first-order with a supercooling follows; The gravitational waves are generated at much lower temperature (T_*) than critical temperature T_{cr} at which the broken and symmetric vacua equilibrate. One might be skeptical of using the daisy improved potential for a system at $T = T_* \ll T_{\text{cr}}$ because it partly includes the high-temperature expression of Eq. (28). This problem was addressed in the recent work [40] in a different model of the conformal symmetry breaking, and the daisy improved potential was consistent with the potential derived without recourse to high-temperature assumption at $T \sim T_*$, as long as the high temperature expansion is not performed for the thermal function J_B . Therefore, we assume the applicability of the daisy improvement at $T = T_*$ and provide some discussions in Sec. IV C.

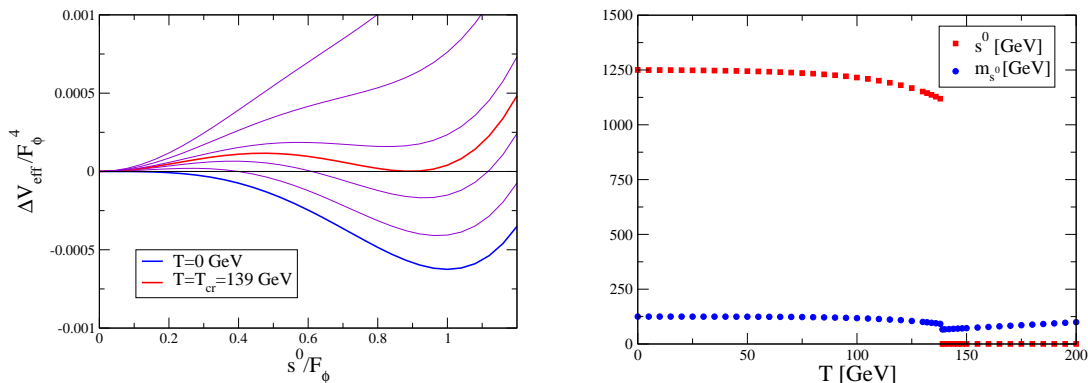


FIG. 2: (Left) Effective potential ($\Delta V_{\text{eff}} \equiv V_{\text{eff}}(s^0, T) - V_{\text{eff}}(0, T)$) for various temperature. The red and blue lines represent the potential at $T = T_{\text{cr}} = 139$ GeV and zero temperature, respectively. (Right) The vev (s^0) (red squares) and dilaton mass m_{s^0} (blue circles) determined at the potential minimum as a function of temperature.

In the left panel of Fig. 2, we show our effective potential for various temperature with the benchmark value of the dilaton decay constant: $F_\phi = 1.25$ TeV. The zero temperature potential (blue line) is well-defined (no negative mass in logarithm) for any value of s^0 and flat (zero curvature) near the origin. This is a typical feature of the dilaton-type potential and contrasted sharply with a usual one loop potential with a negative mass squared at classical level. The

potential monotonically decreases till the minimum and does not possess any barrier at $T = 0$. This property persists at finite temperature unless it exceeds a small threshold value. Therefore, in the cooling and expanding universe, the symmetric phase does not survive in the end, and the cosmological phase transition should complete at certain temperature. Thus, our model does not suffer from the graceful-exit problem which is recently discussed in the context of the first-order electroweak phase transition [48].

With increasing temperature, the potential shape evolves to a double-well structure and two vacua get equilibrated at $T = T_{\text{cr}} \simeq 139$ GeV (red line) where the first-order chiral phase transition takes place. The right panel of Fig. 2 shows the corresponding vev (red squares) and dilaton mass (blue circles) as a function of temperature. The strength of the transition is found to be very strong, $\langle s^0(T_{\text{cr}}) \rangle / T_{\text{cr}} \simeq 8.1 \gg 1$, and strong gravitational waves are created and detectable by LISA project as shown in the next section. As mentioned in Sec. II B, the dilaton-type potential in Eq. (11) does not have quadratic negative curvature at the origin and small finite temperature effects immediately create a shallow potential barrier far separating two vacua. Therefore, it naturally follows as a dilaton-like potential that its phase transition becomes strong first-order.

The dilaton mass m_{s^0} (blue points in the right panel) is 125 GeV at $T = 0$, and decreases for larger T in the broken phase, and shows a singular behavior at the critical temperature T_{cr} . In the symmetric phase, m_{s^0} starts increasing due to the thermal mass effects $\Pi(T)$ given in Eq. (28).

IV. BUBBLE NUCLEATION AND THE GRAVITATIONAL WAVE SIGNAL

In this section, we investigate the spectrum of the stochastic gravitational waves $h^2\Omega_{\text{GW}}(f)$, ($h =$ Hubble constant today/100, $f =$ frequency) which results from the first-order phase transition shown in the previous section. In principle, $h^2\Omega_{\text{GW}}(f)$ could be obtained by solving Einstein equation; The matter sector is specified to the energy momentum tensor for the dilaton and the plasma velocity fields with the equation of state derived by the effective potential. However, we do not adopt this strategy but utilize the formulas shown in Appendix B; The f dependence of the $h^2\Omega_{\text{GW}}$ has been known in the literature (see Ref. [49] and references are therein), and the remaining ambiguities are only three bulk parameters (T_* , $\alpha(T_*)$, $\hat{\beta}(T_*)$). Here, T_* denotes the temperature when the gravitational waves are produced. The parameters $\alpha(T_*)$ and $\hat{\beta}(T_*)$ are associated with the latent heat and the bubble nucleation rate at T_* , respectively. In the following subsections, we explicitly define and calculate them by using our effective potential, and compare the obtained gravitational wave spectra with the LISA sensitivity curves.

A. Bubble nucleation with supercooling

The phase transition taking account of the bubble nucleation dynamics in the expanding Universe is referred to as the cosmological phase transition, which has been studied in [50–52]. It is important to calculate the action of the bounce solution of the dilaton field in the early universe, which characterizes the bubble nucleation through the vacuum tunneling. We start from the bubble nucleation probability per unit volume/time (Γ) given by

$$\Gamma = a(T)e^{-S_E(T)}, \quad (30)$$

where $S_E(T)$ is the Euclidean action describing the bubble dynamics at T . At finite temperature, it can be approximately represented as $S_E = S_3/T$, where S_3 is the three dimensional Euclidean action,

$$S_3(T) = \int d^3x \left[\frac{1}{2} (\partial_i s^0(\mathbf{x}, T))^2 + V_{\text{eff}}(s^0(\mathbf{x}, T), T) \right]. \quad (31)$$

The bubble nucleation temperature (T_n) is defined as a temperature at which the nucleation rate Γ normalized by the Hubble expansion rate at finite temperature $H(T)$ becomes order 1: $\Gamma(T_n)/H^4(T_n) \sim 1$. Since the prefactor $a(T)$ in Eq. (30) is proportional to T^4 , the nucleation condition is rewritten as

$$\frac{S_3(T_n)}{T_n} \simeq 4 \log \left[\frac{T_n}{H(T_n)} \right] \sim 140, \quad (32)$$

where,

$$H(T) = \frac{8\pi G_N}{3} \rho_{\text{rad}}(T), \quad \rho_{\text{rad}}(T) = \frac{\pi^2 T^4 g_*(T)}{30}, \quad (33)$$

with G_N and $g_*(T)$ being the Newton constant and the effective degrees of freedom in the plasma, respectively. We will find $T_n \ll T_{\text{cr}}$ and only SM degrees of freedom are active at $T = T_n$: $g_*(T_n) = 106.75$. In Eq. (32), the logarithm term is solely determined by the Newton constant G_N and almost independent of T , and thus approximated as 140 as indicated by the second equality [47].

We assume the gravitational waves are created at the bubble nucleation temperature $T_* = T_n$. From the fact that the universe is expanding, the nucleation temperature T_n becomes smaller than the critical temperature T_{cr} at which the phase transition sets in (two vacua equilibrate). This is particularly true for the strong first-order phase transition where a strong supercooling holds ($T_* = T_n \ll T_{\text{cr}}$). We note that a refined estimate of T_* is found in the recent development [48].

As shown in Appendix B, the gravitational wave spectrum is characterized by T_* and two additional parameters ($\alpha(T_*), \tilde{\beta}(T_*)$). The parameter α represents a normalized latent heat ($\Delta\epsilon(T)$),

$$\alpha(T) = \frac{\Delta\epsilon(T)}{\rho_{\text{rad}}(T)}, \quad (34)$$

where the radiation energy density ρ_{rad} is defined in Eq. (33). The latent heat $\Delta\epsilon$ is calculated from the effective potential as

$$\Delta\epsilon(T) = -\Delta V_{\text{eff}}(T) + T \frac{d}{dT} \Delta V_{\text{eff}}(T), \quad (35)$$

where $\Delta V_{\text{eff}}(T)$ is the difference of the effective potential at true and false vacua. Needless to say, $\Delta\epsilon$ can be defined when two vacua coexists. A stronger first-order phase transition results in a larger latent heat, and thereby, a stronger gravitational wave signal.

Another parameter $\tilde{\beta}$ is related to the expansion coefficient of (S_3/T) around the bubble nucleation time $t = t_n = t_*$,

$$(S_3/T)_t \simeq (S_3/T)_{t_*} - \beta(t - t_*), \quad \beta = -\left. \frac{d(S_3/T)}{dt} \right|_{t=t_*}. \quad (36)$$

By definition, β measures how rapidly a bubble nucleates. In the expanding Universe, the normalized β ,

$$\tilde{\beta}(T_*) \equiv \frac{\beta}{H(T_*)} = T_* \left. \frac{d}{dT} \left(\frac{S_3}{T} \right) \right|_{T=T_*}. \quad (37)$$

is the relevant measure. The parameter $\tilde{\beta}(T_*)$ combined with T_* determines the peak frequency of the gravitational wave spectrum.

In order to obtain $\tilde{\beta}(T_*)$, one must determine the spatial dilaton field configuration $s^0(\mathbf{x})$ and evaluate the three dimensional effective action S_3/T given by Eq. (31). We assume the spherical configuration $s^0(r)$ with $r = \sqrt{x^2 + y^2 + z^2}$. The relevant configuration is the bounce solution of the equation of motion derived from Eq. (31),

$$\frac{d^2 s_b^0(r, T)}{dr^2} + \frac{2}{r} \frac{ds_b^0(r, T)}{dr} - \frac{dV_{\text{eff}}(s_b^0, T)}{ds_b^0} = 0, \quad (38)$$

with the boundary condition of

$$\left. \frac{2}{r} \frac{ds_b^0(r)}{dr} \right|_{r=0} = 0, \quad s_b^0(r)|_{r=\infty} = 0. \quad (39)$$

Here, $r = 0$ correspond to the center of the bubble. We obtain the bounce solution numerically by using the overshooting/undershooting method. By tuning T , we obtain the bounce action $S_3(T)$ at $T = T_*$, which satisfies the condition of Eq. (32).

In the left panel of Fig. 3, we plot the bounce solution of the differential equation Eq. (38) for $F_\phi = 1250$ GeV. Each line shows a solution at different temperature. The orange line is the highest temperature solution in the figure, and the large portion of $s_b^0(r)$ distributes at small r , indicating a small bubble. As the Universe cools down, the $s_b^0(r)$ gradually distributes at larger r . We find the bounce solution which satisfies the nucleation condition Eq. (32) when temperature becomes $T = T_* = 11.15$ GeV (red line), at which the gravitational waves are created. Thus, the strong supercooling $T_* \ll T_{\text{cr}} = 139$ GeV holds. At smaller temperature, the bounce solution extends to a larger r region as shown by the navy line. In the right panel, $((S_3/T) - 140)$ is plotted as a function of temperature T . The vanishing point is found at $T = T_* = 11.15$ GeV, where the slope multiplied by T_* gives the parameter $\tilde{\beta}$ defined in Eq. (37).

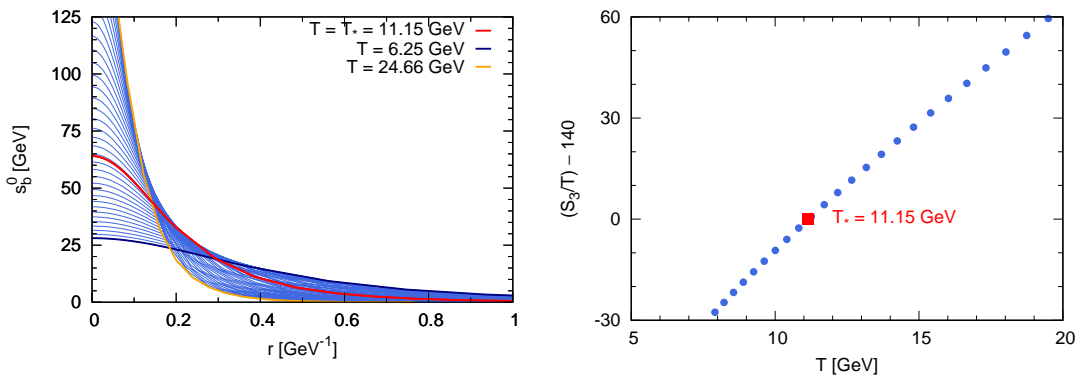


FIG. 3: (Left) Bounce solution in Eq. (38). Each line shows a solution at different temperature. The red line corresponds to the solution which satisfies the nucleation condition Eq. (32). (Right) The $(S_3/T) - 140$ as a function of temperature T . The vanishing point at $T = T_* = 11.15$ is associated with the red line in the left panel.

We summarize the results for $(T_*/F_\phi, \alpha, \tilde{\beta})$:

$$\begin{aligned} (T_*/F_\phi, \alpha, \tilde{\beta}) &= (0.025, 69.5, 128.1) , & (F_\phi = 1000 \text{ GeV}) , \\ (T_*/F_\phi, \alpha, \tilde{\beta}) &= (0.009, 2811.6, 87.5) , & (F_\phi = 1250 \text{ GeV}) . \end{aligned} \quad (40)$$

In Ref. [49], the benchmark values of $(\alpha, \tilde{\beta})$ are shown for various models. Most of models give $\alpha \lesssim \mathcal{O}(0.1)$. In comparison, our α is much larger, particularly for $F_\phi = 1250$ GeV, and thus the strong gravitational wave signal is expected. The obtained $\tilde{\beta}$ is in the middle range while the T_* is very small. As a result, the peak frequency of the gravitational waves becomes small and found to meet the LISA best sensitivity region.

B. Numerical results of gravitational wave spectrum

In the cosmological first-order phase transition, the gravitational wave signal $h^2\Omega_{\text{GW}}$ is known to be created via the three processes, that is, the broken phase bubble collisions, the sound waves in the plasma, and the magnetohydrodynamics (MHD) turbulence in the plasma. The corresponding spectra are denoted as $h^2\Omega_\phi$, $h^2\Omega_{\text{sw}}$, and $h^2\Omega_{\text{turb}}$, respectively, and the formulas to calculate them are summarized in Appendix B.

The scalar contribution $h^2\Omega_\phi$ is dictated by the bubble wall velocity (v_w). Until the recent development [53], it was usually assumed that the bubble walls in the strong first-order transition can be accelerated without bound and run away with the speed of light ($v_w \rightarrow 1$, the runaway bubbles in vacuum) [54] and the $h^2\Omega_\phi$ could have a significant contribution to the total spectrum $h^2\Omega_{\text{GW}}$. However, more advanced study [53] argues that the higher-order corrections to the friction term prevent the bubble wall from becoming runaway, and the runaway bubbles seem unlikely in the thermal phase transition [55, 56]. For the strong phase transition with a large value of $\alpha > 1$, the bubble velocity is still approximated by the speed of light $v_w \simeq 1$ but considered as a *non-runaway* for which the scalar contribution $h^2\Omega_\phi$ is no longer the dominant source of the gravitational wave signals (see e.g. [40, 57]). We assume that this is the case since we have obtained a large value of $\alpha \gg 1$ with strong supercooling (see Eq. (40)).

The dominant source now becomes the sound wave contributions $h^2\Omega_{\text{sw}}$ which arise from the fluid dynamics [58–62]. As seen in Eq. (B4), $h^2\Omega_{\text{sw}}$ is characterised by the fraction (κ_v) of the released latent heat that goes to the plasma bulk motion. In our case with non-runaway bubbles whose velocity is close to the runaway, κ_v is approximately given as

$$\kappa_v \simeq \alpha(0.73 + 0.083\sqrt{\alpha} + \alpha)^{-1} , \quad (41)$$

for $\alpha > 1$ [63]. The gravitational waves for a smaller v_w with $\alpha \lesssim \mathcal{O}(1)$ will also be studied in the next subsection by using the modified expression of κ_v .

For the turbulence contribution $h^2\Omega_{\text{turb}}$, we use a form modeled by [64, 65] based on the Kolmogorov-type turbulence [66]. The parameter κ_{turb} in Eq. (B6) describes the fraction of the released latent heat that goes to the turbulent motion of the plasma. A numerical simulation suggests $\kappa_{\text{turb}} \sim \epsilon\kappa_v$ with $\epsilon = 0.05 - 0.1$ [59], and we adopt $\epsilon = 0.05$ in our analysis.

Fig. 4 presents our results for the gravitational wave signals from the contributions of the sound waves and MHD turbulence in $N_f = 8$ case for two values of $F_\phi = 1000$ GeV (left) and 1250 GeV (right) favored in the walking technicolor model [8]. The peaks locate around $10^{-4} - 10^{-3}$ Hz, where the dominant contributions come from the sound waves and the strength ($h^2\Omega_{\text{GW}}$) exceeds 10^{-8} . The small MHD contributions simply result from using a small value of the fraction $\epsilon = 0.05$. At large frequency ($f \gg f_{\text{turb}}$), the slope in MHD is determined by the Kolmogorov turbulence model with the power-law scaling $\sim f^{-5/3}$ while the asymptotic scaling of the sound wave behaves as $\sim f^{-4}$ ($f \gg f_{\text{sw}}$). As a result, the MHD eventually dominates at large f . The important region comparable to the LISA experiments is $f \sim 10^{-4} - 10^{-2}$ Hz, thus the sound waves plays a crucial role.

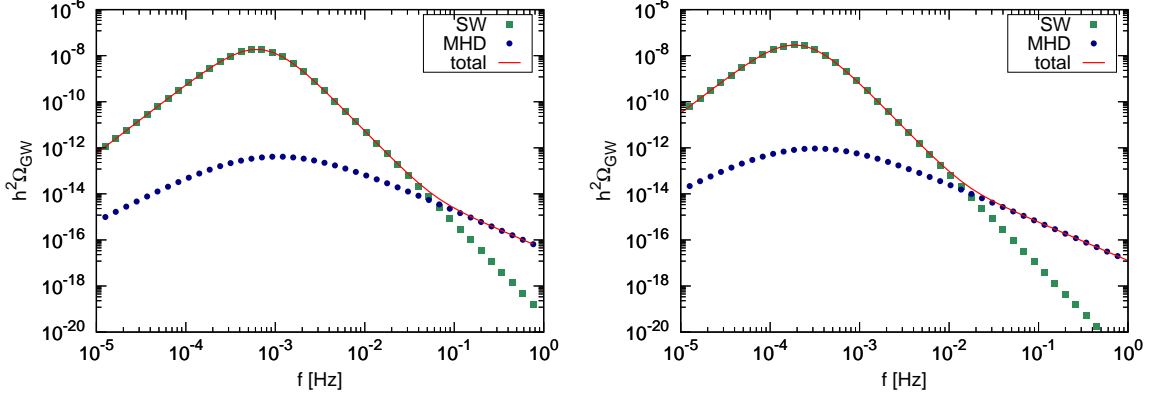


FIG. 4: Gravitational wave signal from sound waves (green squares) and MHD turbulence (navy circles). The red solid line represents the total of them. Left/Right: $F_\phi = 1000$ GeV/ $F_\phi = 1250$ GeV.

In Fig. 5, we show our gravitational wave signals for the total contributions (sound waves + MHD turbulence) and compare them with LISA sensitivities expected in four representative configurations (C1 - C4) [49]. In $F_\phi = 1000$ GeV (left panel), our gravitational spectrum achieves very strong signals detectable in all (C1 - C4) LISA configurations. The strong signal is a characteristic feature of the Gildener-Weinberg type potential with a scale symmetry. In $F_\phi = 1250$ GeV (right panel), the strength of the signal gets slightly larger than the $F_\phi = 1000$ GeV case and the peak position is shifted to somewhat smaller frequency region. The signal has a large overlap to LISA sensitivities again. The peak shift comes from a smaller nucleation temperature with a stronger phase transition at larger F_ϕ . Interestingly, the particular choices of F_ϕ motivated by the walking technicolor model result in peaks close to the most sensitive frequency region in LISA.

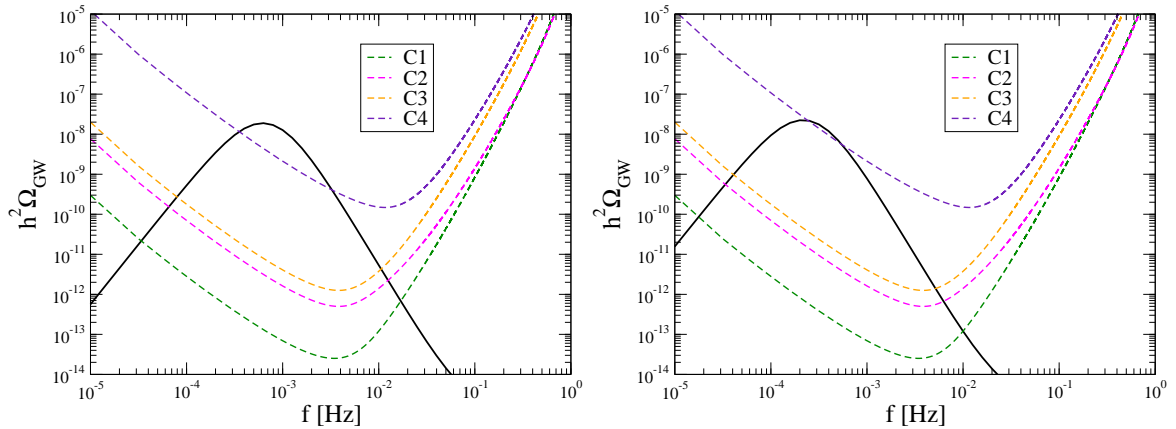


FIG. 5: Gravitational wave signal (black solid line) compared with LISA sensitivities for configurations C1 - C4 (dashed lines) [49]. Left/Right: $F_\phi = 1000$ GeV/ $F_\phi = 1250$ GeV.

C. Discussion

In the previous section, we have shown that the dilaton-type potential leads to the strong gravitational wave signal detectable in the LISA project. We have also mentioned that the results are not affected at all by the pseudoscalar mass term $(\Delta m_p)^2$ which is responsible for a large mass hierarchy between the dilaton and the other spectra. Strictly speaking, however, the heavy spectra might partly stem from another soft breaking mass term for flavor-non-singlet scalar:

$$V_{\text{soft}}^{(s)} = \frac{(\Delta m_s)^2}{2} \sum_{i=1}^{N_f^2-1} (s^i)^2. \quad (42)$$

The mass term respects the massless feature of the dilaton (no $(s^0)^2$ term) at classical level. Combining Eq. (42) with the pseudoscalar mass term Eq. (20), the s^0 -dependent mass functions at tree level reads,

$$\begin{aligned} m_{s^0}^2(s^0, \Delta m_p, \Delta m_s) &= 0, & m_{s^i}^2(s^0, \Delta m_p, \Delta m_s) &= (\Delta m_s)^2 + \frac{2f_2}{N_f}(s^0)^2, \\ m_{p^a}^2(s^0, \Delta m_p, \Delta m_s) &= (\Delta m_p)^2. \end{aligned} \quad (43)$$

In contrast to $(\Delta m_p)^2$, $(\Delta m_s)^2$ gives an additive correction to the dilaton field s^0 term in the field dependent mass term of flavor-non-singlet scalar $m_{s^i}^2$, and affects the phase transition dynamics and gravitational wave spectra. The details of the mass spectra at one loop with $(\Delta m_s)^2$ are summarized in Appendix A. Using Eq. (43), the total effective potential becomes,

$$\begin{aligned} V_{\text{eff}}(s^0, \Delta m_p, \Delta m_s, T) &= \frac{N_f^2 - 1}{64\pi^2} \mathcal{M}_{s^i}^4(s^0, \Delta m_p, \Delta m_s, T) \left(\ln \frac{\mathcal{M}_{s^i}^2(s^0, \Delta m_p, \Delta m_s, T)}{\mu_{\text{GW}}^2} - \frac{3}{2} \right), \\ &+ \frac{T^4}{2\pi^2} (N_f^2 - 1) J_B(\mathcal{M}_{s^i}^2(s^0, \Delta m_p, \Delta m_s, T)/T^2) + C(T), \end{aligned} \quad (44)$$

with,

$$\mathcal{M}_{s^i}^2(s^0, \Delta m_p, \Delta m_s, T) = m_{s^i}^2(s^0, \Delta m_p, \Delta m_s) + \Pi(T), \quad (45)$$

where the thermal mass $\Pi(T)$ is given in Eq. (28).

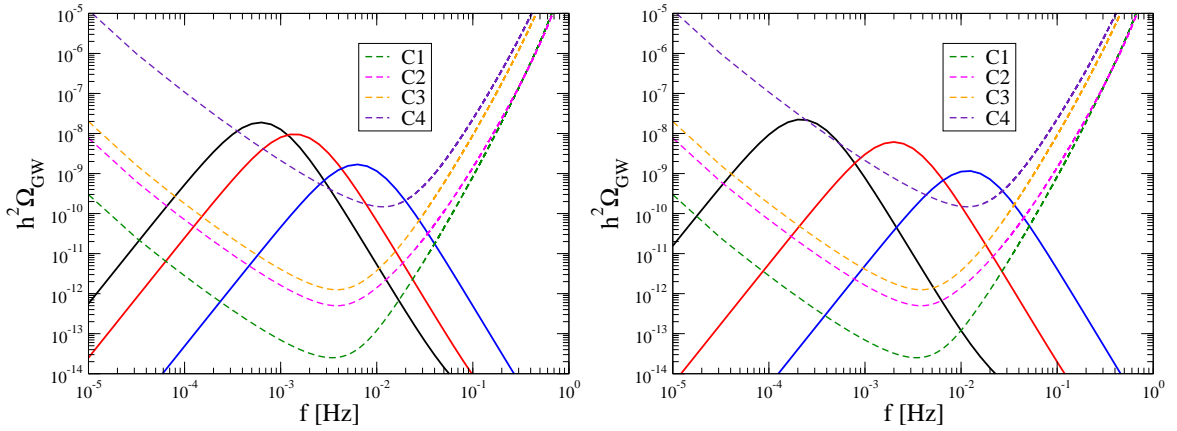


FIG. 6: The soft breaking scalar mass $(\Delta m_s)^2$ effects to the gravitational wave spectra for $F_\phi = 1000$ GeV (left) and $F_\phi = 1250$ GeV (right). The black, red, and blue colored solid curves represent the results with $(\Delta m_s)^2/F_\phi^2 = 0, 0.0001, \text{ and } 0.001$, respectively. The dashed lines represent the LISA sensitivity curves.

In Fig. 6, we show the gravitational wave spectra obtained by using Eq. (44) with $(\Delta m_s)^2/F_\phi^2 = 10^{-4}$ (solid-red) and $(\Delta m_s)^2/F_\phi^2 = 10^{-3}$ (solid-blue), and compare them to the result with $\Delta m_s = 0$ (solid-black) and the LISA sensitivity curves (dashed-lines). In both $F_\phi = 1000$ GeV (left) and 1250 GeV (right) cases, the peak positions are shifted to the larger frequency region and the strength becomes somewhat smaller due to the scalar mass perturbations. However,

$(\Delta m_s)^2/F_\phi^2$	Δm_s [GeV]	T_* [GeV]	f_{peak} [Hz]	$h^2\Omega_{\text{GW}} _{\text{peak}}$
0.0	0.0	11.5	1.9×10^{-4}	3.0×10^{-8}
0.0001	12.5	25.8	2.0×10^{-3}	6.1×10^{-9}
0.001	39.5	52.9	1.2×10^{-2}	1.3×10^{-9}
0.01	125.0	111.3	1.1×10^{-1}	1.4×10^{-11}
0.02	176.8	137.5	3.4×10^{-1}	1.5×10^{-12}
0.03	216.5	154.8	6.3×10^{-1}	3.2×10^{-13}
0.04	250.0	168.0	9.9×10^{-1}	9.3×10^{-14}
0.05	279.5	178.6	3.7	1.1×10^{-14}

TABLE I: Summary table of the peak frequencies and the strength of the gravitational wave signals at peak as well as the nucleation temperature ($F_\phi = 1250$ GeV case).

the qualitative feature is not changed from the case with $\Delta m_s = 0$; The signals are still very strong and detectable even in the severe constraint case of C4. Thus, the strong gravitational wave signal is not spoiled by the small $(\Delta m_s)^2$ perturbation. This is somewhat surprising because our model relying on the scale symmetry looks sensitive to infinitesimal mass perturbation but it seems not happening in our model. We can understand this as follows; The gravitational waves are generated at T_* much smaller than the critical temperature T_{cr} , and the effective potential in the broken vacuum at T_* is close to the zero temperature potential. Then, in the mass function Eq. (45), the dominant scale in the broken vacuum is $\langle s^0 \rangle \sim F_\phi$ and $(\Delta m_s)^2$ is negligible. In the symmetric vacuum, the s^0 dependent part disappears in Eq. (45) but the thermal mass $\Pi(T)$ protects the system from $(\Delta m_s)^2$. In fact, $(\Delta m_s)^2 < \Pi(T_*)$ is satisfied for small $(\Delta m_s)^2/F_\phi^2 = 10^{-4}$ and 10^{-3} as shown in Table I. Thus, $(\Delta m_s)^2$ is subdominant in both symmetric and broken vacua.

We extend our study for a larger mass perturbation $(\Delta m_s)^2$ comparable or larger than the thermal mass $\Pi(T)$. It is important to know the threshold of $(\Delta m_s)^2$ below which the first-order phase transition survives. This is the subject of the tri-critical point (TCP) in the the phase diagram in $T - \Delta m_s$ plane, which we provide in Fig. 7 for $F_\phi = 1250$ GeV. It is convenient to consider two auxiliary curves C_2 and C_4 which are defined as a pair of Δm_s and T satisfying:

$$C_2 : \left. \frac{\partial^2 V_{\text{eff}}(s^0, \Delta m_p, \Delta m_s, T)}{(\partial s^0)^2} \right|_{s^0 \rightarrow 0} = 0, \quad C_4 : \left. \frac{\partial^4 V_{\text{eff}}(s^0, \Delta m_p, \Delta m_s, T)}{(\partial s^0)^4} \right|_{s^0 \rightarrow 0} = 0. \quad (46)$$

The curve C_2 is equivalent to the phase boundary in the second-order region (blue solid line) which appears at large Δm_s region. The crossing point of C_2 and C_4 corresponds to TCP at which the first-order phase boundary (red solid line) terminates. As shown in the phase diagram, the TCP is found at $(\Delta m_{s,\text{TCP}}, T_{\text{TCP}}) = (424, 222)$ GeV in our model. We select $(\Delta m_s)^2/F_\phi^2 = 0.01 - 0.05 < \Delta m_{s,\text{TCP}}^2/F_\phi^2 \simeq 0.115$ and investigate the gravitational waves in approaching to TCP from first-order transition side. The nucleation temperature T_* should exist between the first-order phase boundary and C_2 . As shown by the red squares (see Table I for the numerics), T_* locates near the C_2 and the bubble nucleation is found to happen just before the potential barrier disappears in the cooling Universe.

In approaching to TCP, the supercooling strength (distance between T_* and red line) diminishes, which indicates a gravitational wave signal getting weaker. However, before reaching at TCP, we find that the spectral peak position meets the DECIGO target frequencies (~ 0.1 Hz) [24, 25] as shown in Table I. Depending on the DECIGO configurations, three sensitivity curves are considered in Ref. [69] (one of three curves called ‘‘original’’ is found in [70]). The maximal sensitivities allows us to detect the signal of $h^2\Omega_{\text{GW}} \sim \mathcal{O}(10^{-15})$ around $0.2 - 2.0$ Hz. For $(\Delta m_s)^2/F_\phi^2 = 0.01 - 0.04$ (except 0.05), our results $h^2\Omega_{\text{GW}} \sim \mathcal{O}(10^{-11} - 10^{-13})$ are much larger than at least one of the three sensitivity curves in the corresponding frequency region and would be detectable in DECIGO.

As explained in the previous section, we have so far assumed that the wall velocity is close to the speed of light $v_w \simeq 1$. This assumption is valid for a large latent heat $\alpha(T_*) > \mathcal{O}(1)$ while it becomes $\mathcal{O}(0.1 - 1)$ for $(\Delta m_s/F_\phi)^2 \geq 0.01$. Therefore, we have checked the gravitational wave spectrum by using slightly smaller than the speed of sound: $v_w \lesssim v_s = 1/\sqrt{3}$. In this case, the released latent heat fraction κ_v given in Eq. (41) must be modified as [63, 71]

$$\kappa_v \simeq \frac{v_s^{11/5} \kappa_a \kappa_b}{(v_s^{11/5} - v_w^{11/5}) \kappa_b + v_s^{6/5} v_w \kappa_a}, \quad (47)$$

where, $\kappa_a \simeq 6.9\alpha v_w^{6/5}/(1.36 - 0.037\sqrt{\alpha} + \alpha)$ and $\kappa_b \simeq \alpha^{2/5}/(0.017 + (0.997 + \alpha)^{2/5})$. Comparing to the results shown in Table I, the peak frequency f_{peak} becomes 1.7 times larger but still in the DECIGO sensitivity region. The spectra

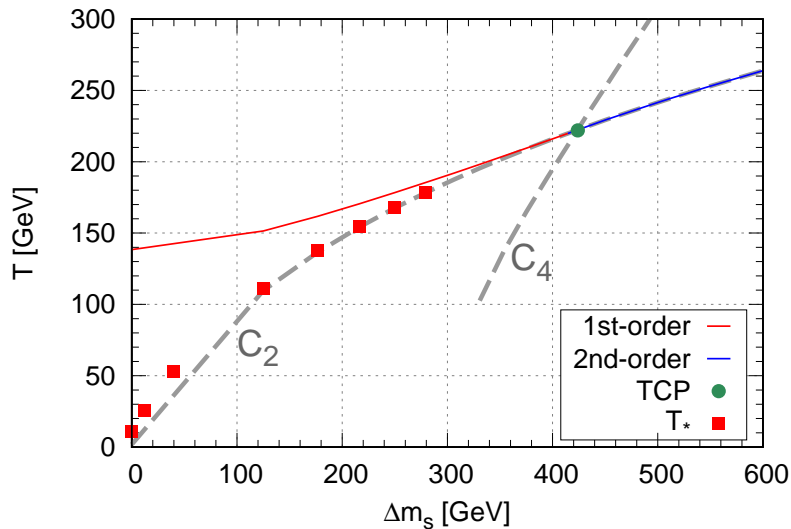


FIG. 7: Phase diagram for the chiral phase transition and the nucleation temperature T_* when including the soft breaking scalar mass Δm_s .

at f_{peak} are enhanced by a factor $1.4 - 3.2$ for $(\Delta m_s/F_\phi)^2 = 0.01 - 0.04$. Therefore, the detectability in DECIGO remains intact for $v_w \lesssim v_s$ and does not depend on the details of v_w .

Finally, we discuss the limitation of the daisy improved effective potential which we have adopted. In the recent work [40], it was shown that the daisy improved potential was close to the one derived by solving a gap equation without high temperature assumptions for the self-energy, even at $T \sim T_* \ll T_{\text{cr}}$. This would be understandable as follows; In the broken vacuum at $T_* \ll T_{\text{cr}}$, the thermal effects are negligible and whatever the daisy or more sophisticated one does not matter, and in the symmetric vacuum, nucleation temperature T_* is considered to be *high* in the sense that T_* is larger than mass scales in the symmetric phase, and the daisy improvement becomes a good approximation there. However, this is not true anymore in the vicinity of the TCP, and the results in this work at large Δm_s might suffer from this problem. In this regard, the gravitational waves near TCP should be further investigated beyond the daisy diagram near future.

V. CONCLUSION

The walking technicolor model, having a large anomalous dimension $\gamma_m \simeq 1$ and a composite Higgs as a pseudo dilaton (“technidilaton”) of the approximate scale symmetry [1, 2], is a viable candidate for physics beyond the Standard Model. Considering the early Universe at high temperature, the walking technicolor model is expected to undergo a strong first-order electroweak phase transition characteristic to the Coleman-Weinberg (CW) type dilaton potential due to the scale symmetric nature. Remarkably enough, the spectrum of stochastic gravitational waves $h^2\Omega_{\text{GW}}(f)$ from the first-order transition could be observed in LISA and DECIGO experiments in the coming years. In this regard, we have examined the $h^2\Omega_{\text{GW}}(f)$ from the walking technicolor by using the linear sigma model with classical scale symmetry which simulates the scale symmetric nature of the walking technicolor. As a bench mark model as such, we took the “one-family model” with $N_f = 8$ (four electroweak doublets) in the QCD-like $SU(N_c)$ gauge theory (Lattice studies revealed that $N_f = 8$, $N_c = 3$ is a walking theory with a light flavor-singlet scalar [15–18]).

Thus our linear sigma model has the chiral $U(N_f)_L \times U(N_f)_R$ symmetry together with the scale symmetry at classical level particularly for $N_f = 8$ as a bench mark walking technicolor. The scale and chiral symmetries are spontaneously broken at one loop level through the Coleman-Weinberg (CW) mechanism à la Gildener-Weinberg [34], where the scalar in the ray direction (“scalon”) is nothing but a light pseudo dilaton (techni-dilaton) to be identified with the 125 GeV Higgs particle. We have shown that our CW potential is equivalent to the most general dilaton potential derived as the effective theory of the walking technicolor model [26]. Based on the equivalence, the vacuum expectation value (vev , $\langle s^0 \rangle$) is identified with the dilaton decay constant F_ϕ rather than the usual linear sigma model restriction $v_{\text{EW}} = \sqrt{N_f/2}F_\pi = 246$ GeV. For $F_\phi = 1.25$ TeV preferred by the walking technicolor model [8], we have

found the coupling constant $f_2^2 \simeq (0.45)^2 \ll 1$ and thus the one loop perturbation theory is justified. In addition, the radiative corrections from the SM particles can be subdominant and neglected owing to the large value of F_ϕ .

We have introduced a soft chiral symmetry breaking by the pseudoscalar mass term $(\Delta m_p)^2$ given in Eq. (20) to mock up the NG bosons masses of flavor-non-singlet pseudoscalar ($p^{i=1-63} = \pi^i = \text{NG-pions}$) generated from the gauge interactions of the ETC, and the Standard Model $SU(3) \times SU(2) \times U(1)$, and η' mass by the chiral anomaly. This also results in the mass hierarchy between the light pseudo dilaton (flavor-singlet scalar, s^0) and the other massive scalars: flavor-non-singlet scalar ($s^{i=1-63} = a_0^i$). At one loop level this breaking happens not to shift the mass of the pseudo dilaton consistently with the PCDC relation.

In order to investigate the thermal phase transition in our model, we have considered the one loop thermal effective potential with a daisy diagram improvement. Due to the scale symmetric feature of our CW potential, we have observed a very strong first-order electroweak phase transition which is not affected by the soft mass term given in Eq. (20) at all. We have shown that the barrier between the symmetric and the broken vacua disappears at temperature below a small finite threshold, so that our model does not suffer from the graceful-exit problem which is recently discussed in the context of the first-order electroweak phase transition [48].

In order to investigate the gravitational waves from the resultant first-order phase transition, we have numerically examined the bounce solution for the effective action describing the bubble nucleation dynamics. We have found a strong supercooling ($T_* \ll T_{\text{cr}}$), large latent heat $\alpha(T_*) \gg 1$, and the nucleation rate parameter $\tilde{\beta}(T_*) \sim \mathcal{O}(10^2)$. The results are summarized in Eq. (40). (See Sec. IV A for the parameter definition).

For the given $(T_*, \alpha(T_*), \tilde{\beta}(T_*))$, the stochastic gravitational wave spectrum $h^2\Omega_{\text{GW}}$ is evaluated by using the formulas shown in Appendix B. For the dilaton decay constant $F_\phi = 1000$ GeV and 1250 GeV, we have obtained very strong gravitational wave signals $h^2\Omega_{\text{GW}}(f) \sim 10^{-8}$ near the best sensitivity frequency region ($f \simeq 10^{-3}$ Hz) of the LISA experiment and the signals are detectable in all (C1 - C4) representative configurations [49].

We also have discussed the effect of the possible additional soft mass term $(\Delta m_s)^2$ for the flavor non-singlet scalar given in Eq. (42). Similarly to the pseudoscalar mass term $(\Delta m_p)^2$ mentioned above, the $(\Delta m_s)^2$ term preserves the massless feature of the pseudo dilaton at classical level and contributes to the mass hierarchy between the pseudo dilaton and the other spectra. Unlikely to $(\Delta m_p)^2$, however, the finite $(\Delta m_s)^2$ modifies the phase transition dynamics in general.

For $(\Delta m_s/F_\phi)^2 = 10^{-4}$ and 10^{-3} , which are smaller than the thermal mass $\Pi(T)/F_\phi^2$, the gravitational wave signals are still very strong and detectable in all (C1 - C4) configurations [49]. For larger Δm_s , we have considered the phase diagram in $\Delta m_s - T$ plane for $F_\phi = 1250$ GeV, and located the tri-critical point (TCP: $(\Delta m_{s,\text{TCP}}, T_{\text{TCP}}) = (424, 222)$ GeV). Approaching to TCP from the first-order region, the gravitational wave signal becomes weaker, but before reaching at TCP, the spectral peak position meets the DECIGO target frequencies (~ 0.1 Hz) [24, 25]. The gravitational wave signals for $\Delta m_s = 125 - 250$ GeV would be detectable at least one of three sensitivity curves of DECIGO [69]. The peak frequencies and strengths are summarized in Table I.

Finally, we notice several issues which should be studied in future. First, it is important to refine the effective potential beyond daisy diagram resummation. In particular, the difference between the daisy improved and more sophisticated potentials (e.g. Ref. [40, 67]) may become significant in the vicinity of the TCP. Second, we need to refine the estimate of T_* ; We have assumed that the gravitational waves are produced at the nucleation temperature $T_* = T_n$, while it is argued that T_* is more reasonably determined by the reheating temperature (T_{reh}) rather than T_n in the strong first-order phase transition [48]. Although our results shown in this work might be modified quantitatively by the refinements, the qualitative feature - very strong gravitational wave signals attributed to the scale symmetry of walking technicolor model - would be robust. This suggests that the walking technicolor model could be probed via the gravitational waves near future in LISA and DECIGO experiments.

Acknowledgments

This work is supported in part by JSPS KAKENHI Grant Number 17K14309.

Appendix A: Flavor non-singlet scalar mass

Consider the effective potential in the presence of flavor non-singlet scalar mass $(\Delta m_s)^2$ defined in Eq. (42) at zero temperature,

$$V_{\text{eff}} = \frac{N_f^2 - 1}{64\pi^2} m_{s^i}^4(s^0, \Delta m_p, \Delta m_s) \left(\ln \frac{m_{s^i}^2(s^0, \Delta m_p, \Delta m_s)}{\mu_{\text{GW}}^2} - \frac{3}{2} \right) + C, \quad (\text{A1})$$

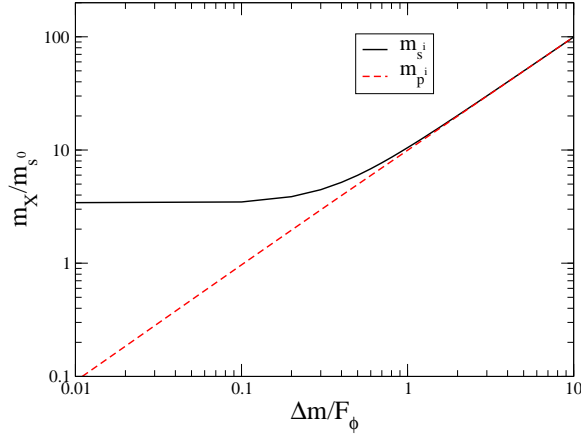


FIG. 8: The $\Delta m = \Delta m_s = \Delta m_p$ dependent mass ratio for $N_f = 8$ with $f_2 = 0.45$.

where C is a constant. The vev for s^0 is obtained from the stationary condition of the effective potential, which for non zero value reads

$$\ln \frac{m_{s^i}^2(\langle s^0 \rangle, \Delta m_s)}{\mu_{GW}^2} = 1 \quad \Rightarrow \quad \langle s^0 \rangle^2 = \frac{N_f}{2f_2} (e\mu_{GW}^2 - (\Delta m_s)^2). \quad (\text{A2})$$

From the result, the value of the explicit breaking mass $(\Delta m_s)^2$ should satisfy the condition $(\Delta m_s)^2 < e\mu_{GW}^2$ for the spontaneous symmetry breaking.

The mass spectra in the presence of $(\Delta m_s)^2$ in terms of $\langle s^0 \rangle$ are given as

$$\begin{aligned} m_{s^0}^2 &= \frac{f_2^2}{2\pi^2} \frac{N_f^2 - 1}{N_f^2} \langle s^0 \rangle^2 = \frac{f_2}{4\pi^2} \frac{N_f^2 - 1}{N_f} (e\mu_{GW}^2 - (\Delta m_s)^2) \\ m_{s^i}^2 &= (\Delta m_s)^2 + \frac{2f_2}{N_f} \langle s^0 \rangle^2 + \frac{f_2}{32\pi^2} \left\{ 2N_f (\Delta m_p)^2 \left(\ln \left(\frac{(\Delta m_p)^2}{\mu_{GW}^2} \right) - 1 \right) \right. \\ &\quad \left. + f_2 \langle s^0 \rangle^2 \left(\frac{18}{N_f} + \frac{2}{N_f} \ln \left(\frac{(\Delta m_p)^2}{\mu_{GW}^2} \right) \right) \sum_{j=1}^{N_f^2-1} (d_{jji})^2 \right\} \\ m_{p^0}^2 &= (\Delta m_p)^2 + \frac{4f_2}{32\pi^2} \left(\frac{N_f^2 - 1}{N_f} \right) (\Delta m_p)^2 \left(\ln \left(\frac{(\Delta m_p)^2}{\mu_{GW}^2} \right) - 1 \right) \\ m_{p^i}^2 &= (\Delta m_p)^2 + \frac{f_2}{32\pi^2} \left(2N_f - \frac{4}{N_f} \right) (\Delta m_p)^2 \left(\ln \left(\frac{(\Delta m_p)^2}{\mu_{GW}^2} \right) - 1 \right). \end{aligned} \quad (\text{A3})$$

The relation between the dilaton mass $m_{s^0}^2$ and vev $\langle s^0 \rangle^2$ (first equality in the first line) is not modified by $(\Delta m_s)^2$ (nor $(\Delta m_p)^2$), and the identities given by Eq. (18) with the coupling $f_2 \simeq 0.45$ remain intact. Fig. 8 shows the ratio of the bosons and the Higgs boson in the case of $\Delta m = \Delta m_s = \Delta m_p$. As a result, the much larger mass hierarchy can be obtained for a large value of Δm compared with the case of $\Delta m = 0$.

In addition, the soft breaking mass parameter Δm_s slightly distorts the dilatonic property of the potential:

$$\left. \frac{\partial V_{\text{eff}}}{\partial s^0} \right|_{s^0=0} = 0, \quad \left. \frac{\partial^2 V_{\text{eff}}}{\partial (s^0)^2} \right|_{s^0=0} = \frac{N_f^2 - 1}{8\pi^2 N_f} (\Delta m_s)^2 f_2 \left(\ln \left(\frac{(\Delta m_s)^2}{\mu_{GW}^2} \right) - 1 \right) \lesssim 0, \quad (\text{A4})$$

for $0 \leq (\Delta m_s)^2 < e\mu_{GW}^2$. Thus the negative curvature at the origin is generated, which destabilizes the symmetric vacuum at the origin for large Δm_s even at finite temperature.

Appendix B: Formulas for gravitational waves spectra from first-order phase transitions

It is known that the stochastic gravitational wave spectrum $h^2\Omega_{\text{GW}}$ created in the first-order phase transition in the early Universe consists of three signals coming from different sources [49]:

$$h^2\Omega_{\text{GW}} \simeq h^2\Omega_\phi + h^2\Omega_{\text{sw}} + h^2\Omega_{\text{turb}}. \quad (\text{B1})$$

The first term $h^2\Omega_\phi$ is the gravitational wave signal created by bubble collisions and associated with a kinetic energy of a scalar (dilaton in this work) field. The second term $h^2\Omega_{\text{sw}}$ represents the signal sourced by sound waves in plasma, and the third term $h^2\Omega_{\text{turb}}$ accounts for Magnetohydrodynamic (MHD) turbulence in the plasma forming after the bubbles have collided.

Following [49], we estimate each contribution as follows,

$$h^2\Omega_\phi(f) = 1.67 \times 10^{-5} \tilde{\beta}^{-2} \left(\frac{\kappa_\phi \alpha}{1 + \alpha} \right)^2 \left(\frac{100}{g_*} \right)^{1/3} \left(\frac{0.11 v_w^3}{0.42 + v_w^2} \right) S_\phi(f), \quad (\text{B2})$$

where,

$$S_\phi(f) = \frac{3.8(f/f_\phi)^{2.8}}{1 + 2.8(f/f_\phi)^{3.8}}$$

$$f_\phi = 16.5 \times 10^3 \tilde{\beta} \left(\frac{0.62}{1.8 - 0.1v_w + v_w^2} \right) \left(\frac{T_*}{100 \text{ GeV}} \right) \left(\frac{g_*}{100} \right)^{1/6} \text{ Hz}, \quad (\text{B3})$$

for the scalar contribution, and

$$h^2\Omega_{\text{sw}}(f) = 2.65 \times 10^{-6} \left(\frac{v_w}{\tilde{\beta}} \right) \left(\frac{\kappa_v \alpha}{1 + \alpha} \right)^2 \left(\frac{100}{g_*} \right)^{1/3} S_{\text{sw}}(f) \quad (\text{B4})$$

where,

$$S_{\text{sw}}(f) = (f/f_{\text{sw}})^3 \left(\frac{7}{4 + 3(f/f_{\text{sw}})^2} \right)^{7/2}$$

$$f_{\text{sw}} = 1.9 \times 10^{-5} \text{ Hz} \left(\frac{\tilde{\beta}}{v_w} \right) \left(\frac{T_*}{100 \text{ GeV}} \right) \left(\frac{g_*}{100} \right)^{1/6}, \quad (\text{B5})$$

for the sound waves, and

$$h^2\Omega_{\text{turb}}(f) = 3.35 \times 10^{-4} \left(\frac{v_w}{\tilde{\beta}} \right) \left(\frac{\kappa_{\text{turb}} \alpha}{1 + \alpha} \right)^{3/2} \left(\frac{100}{g_*} \right)^{1/3} S_{\text{turb}}(f) \quad (\text{B6})$$

where

$$S_{\text{turb}}(f) = \frac{(f/f_{\text{turb}})^3}{[1 + (f/f_{\text{turb}})]^{11/3} (1 + 8\pi f/h_*)},$$

$$f_{\text{turb}} = 2.7 \times 10^{-5} \text{ Hz} \left(\frac{\tilde{\beta}}{v_w} \right) \left(\frac{T_*}{100 \text{ GeV}} \right) \left(\frac{g_*}{100} \right)^{1/6} \quad (\text{B7})$$

for the MHD turbulence.

In the above formulas, the parameters $(T_*, \alpha(T_*), \tilde{\beta}(T_*))$ are calculated from the effective potential in Sec. IV A. The bubble wall velocity v_w is specified to be the speed of light $v_w = 1$ or sound $1/\sqrt{3}$. The parameter κ_v and κ_{turb} are explained in Sec. IV B. The value of the parameter κ_ϕ was not considered in this work because we assumed the bubble contribution $h^2\Omega_\phi$ to be negligible for non-runaway bubbles (see Sec. IV B).

[1] K. Yamawaki, M. Bando and K. i. Matumoto, Phys. Rev. Lett. **56**, 1335 (1986).

- [2] M. Bando, K. i. Matumoto and K. Yamawaki, Phys. Lett. B **178**, 308 (1986).
- [3] T. Akiba and T. Yanagida, Phys. Lett. **169B**, 432 (1986).
- [4] T. W. Appelquist, D. Karabali and L. C. R. Wijewardhana, Phys. Rev. Lett. **57**, 957 (1986).
- [5] B. Holdom, Phys. Lett. **150B**, 301 (1985).
- [6] S. Weinberg, Phys. Rev. D **13**, 974 (1976) Addendum: [Phys. Rev. D **19**, 1277 (1979)].
- [7] L. Susskind, Phys. Rev. D **20**, 2619 (1979).
- [8] S. Matsuzaki and K. Yamawaki, JHEP **1512**, 053 (2015) Erratum: [JHEP **1611**, 158 (2016)] [arXiv:1508.07688 [hep-ph]].
- [9] W. E. Caswell, Phys. Rev. Lett. **33**, 244 (1974).
- [10] T. Banks and A. Zaks, Nucl. Phys. B **196**, 189 (1982).
- [11] T. Appelquist, J. Terning and L. C. R. Wijewardhana, Phys. Rev. Lett. **77**, 1214 (1996) [hep-ph/9602385].
- [12] Y. Aoki, T. Aoyama, M. Kurachi, T. Maskawa, K.-i. Nagai, H. Ohki, A. Shibata, K. Yamawaki, T. Yamazaki (the LatKMI Collaboration) Phys. Rev. D **87**, no. 9, 094511 (2013) [arXiv:1302.6859 [hep-lat]].
- [13] T. Appelquist *et al.* [LSD Collaboration], Phys. Rev. D **90**, no. 11, 114502 (2014) [arXiv:1405.4752 [hep-lat]].
- [14] A. Hasenfratz, D. Schaich and A. Veernala, JHEP **1506**, 143 (2015) [arXiv:1410.5886 [hep-lat]].
- [15] Y. Aoki, T. Aoyama, M. Kurachi, T. Maskawa, K. Miura, K.-i. Nagai, H. Ohki, E. Rinaldi, A. Shibata, K. Yamawaki, T. Yamazaki (the LatKMI Collaboration) Phys. Rev. D **89**, 111502 (2014) [arXiv:1403.5000 [hep-lat]].
- [16] Y. Aoki, T. Aoyama, E. Bennett, M. Kurachi, T. Maskawa, K. Miura, K.-i. Nagai, H. Ohki, E. Rinaldi, A. Shibata, K. Yamawaki, T. Yamazaki (the LatKMI Collaboration), Phys. Rev. D **96**, no. 1, 014508 (2017) [arXiv:1610.07011 [hep-lat]].
- [17] T. Appelquist *et al.*, Phys. Rev. D **93**, no. 11, 114514 (2016) [arXiv:1601.04027 [hep-lat]].
- [18] T. Appelquist *et al.* [Lattice Strong Dynamics Collaboration], arXiv:1807.08411 [hep-lat].
- [19] See for a review: E. Farhi and L. Susskind, Phys. Rept. **74**, 277 (1981).
- [20] R. D. Pisarski and F. Wilczek, “Remarks on the Chiral Phase Transition in Chromodynamics,” Phys. Rev. D **29**, 338 (1984).
- [21] E. Witten, Phys. Rev. D **30**, 272 (1984).
- [22] P. A. Seoane *et al.* [LISA Collaboration], arXiv:1305.5720 [astro-ph.CO].
- [23] H. Audley *et al.* (2017), [arXiv:1702.00786].
- [24] N. Seto, S. Kawamura and T. Nakamura, Phys. Rev. Lett. **87**, 221103 (2001) [astro-ph/0108011].
- [25] S. Sato *et al.*, J. Phys. Conf. Ser. **840**, no. 1, 012010 (2017).
- [26] S. Matsuzaki and K. Yamawaki, Phys. Rev. Lett. **113**, no. 8, 082002 (2014) [arXiv:1311.3784 [hep-lat]].
- [27] M. Golterman and Y. Shamir, Phys. Rev. D **94**, no. 5, 054502 (2016) [arXiv:1603.04575 [hep-ph]].
- [28] A. Kasai, K. i. Okumura and H. Suzuki, arXiv:1609.02264 [hep-lat].
- [29] T. Appelquist, J. Ingoldby and M. Piai, JHEP **1707**, 035 (2017).
- [30] M. Hansen, K. Langæble and F. Sannino, Phys. Rev. D **95**, no. 3, 036005 (2017) [arXiv:1610.02904 [hep-ph]].
- [31] Y. Meurice, Phys. Rev. D **96**, no. 11, 114507 (2017) [arXiv:1709.09264 [hep-lat]].
- [32] T. Appelquist *et al.* [LSD Collaboration], arXiv:1809.02624 [hep-ph].
- [33] Y. Chen, M. Huang and Q. S. Yan, JHEP **1805**, 178 (2018) [arXiv:1712.03470 [hep-ph]].
- [34] E. Gildener and S. Weinberg, Phys. Rev. D **13**, 3333 (1976).
- [35] A. J. Paterson, Nucl. Phys. B **190**, 188 (1981).
- [36] K. Tsumura, M. Yamada and Y. Yamaguchi, JCAP **1707**, no. 07, 044 (2017) [arXiv:1704.00219 [hep-ph]].
- [37] L. Marzola, A. Racioppi and V. Vaskonen, Eur. Phys. J. C **77**, no. 7, 484 (2017) [arXiv:1704.01034 [hep-ph]].
- [38] M. Aoki, H. Goto and J. Kubo, Phys. Rev. D **96**, no. 7, 075045 (2017) [arXiv:1709.07572 [hep-ph]].
- [39] D. Croon, V. Sanz and G. White, JHEP **1808**, 203 (2018) [arXiv:1806.02332 [hep-ph]].
- [40] T. Prokopec, J. Rezacek and B. Swiezevska, arXiv:1809.11129 [hep-ph].
- [41] Y. Aoki, T. Aoyama, E. Bennett, M. Kurachi, T. Maskawaa, K. Miura, K.-i. Nagai, H. Ohki, E. Rinaldi, A. Shibata, K. Yamawaki, and T. Yamazaki [LatKMI Collaboration], PoS LATTICE **2015**, 213 (2016) [arXiv:1601.02287 [hep-lat]]; EPJ Web Conf. **175**, 08023 (2018) [arXiv:1710.06549 [hep-lat]].
- [42] V. A. Miransky and K. Yamawaki, Phys. Rev. D **55**, 5051 (1997) Erratum: [Phys. Rev. D **56**, 3768 (1997)] [hep-th/9611142].
- [43] Y. Kikukawa, M. Kohda and J. Yasuda, Phys. Rev. D **77**, 015014 (2008) [arXiv:0709.2221 [hep-ph]].
- [44] S. Weinberg, Phys. Rev. D **9**, 3357 (1974).
- [45] L. Dolan and R. Jackiw, Phys. Rev. D **9**, 3320 (1974).
- [46] D. J. Gross, R. D. Pisarski and L. G. Yaffe, Rev. Mod. Phys. **53**, 43 (1981).
- [47] M. Quiros, hep-ph/9901312.
- [48] J. Ellis, M. Lewicki and J. M. No, arXiv:1809.08242 [hep-ph].
- [49] C. Caprini *et al.*, JCAP **1604**, no. 04, 001 (2016) [arXiv:1512.06239 [astro-ph.CO]].
- [50] S. R. Coleman, Phys. Rev. D **15**, 2929 (1977) Erratum: [Phys. Rev. D **16**, 1248 (1977)].
- [51] C. G. Callan, Jr. and S. R. Coleman, Phys. Rev. D **16**, 1762 (1977).
- [52] A. D. Linde, Nucl. Phys. B **216**, 421 (1983) Erratum: [Nucl. Phys. B **223**, 544 (1983)].
- [53] D. Bodeker and G. D. Moore, JCAP **1705**, no. 05, 025 (2017) [arXiv:1703.08215 [hep-ph]].
- [54] D. Bodeker and G. D. Moore, JCAP **0905**, 009 (2009) [arXiv:0903.4099 [hep-ph]].
- [55] D. J. Weir, Phil. Trans. Roy. Soc. Lond. A **376**, no. 2114, 20170126 (2018) [arXiv:1705.01783 [hep-ph]].
- [56] R. Jinno and M. Takimoto, arXiv:1707.03111 [hep-ph].
- [57] K. Hashino, R. Jinno, M. Kakizaki, S. Kanemura, T. Takahashi and M. Takimoto, arXiv:1809.04994 [hep-ph].
- [58] M. Hindmarsh, S. J. Huber, K. Rummukainen and D. J. Weir, Phys. Rev. Lett. **112**, 041301 (2014) [arXiv:1304.2433 [hep-ph]].

- [59] M. Hindmarsh, S. J. Huber, K. Rummukainen and D. J. Weir, Phys. Rev. D **92**, no. 12, 123009 (2015) [arXiv:1504.03291 [astro-ph.CO]].
- [60] M. Hindmarsh, S. J. Huber, K. Rummukainen and D. J. Weir, Phys. Rev. D **96**, no. 10, 103520 (2017) [arXiv:1704.05871 [astro-ph.CO]].
- [61] J. T. Giblin, Jr. and J. B. Mertens, JHEP **1312**, 042 (2013) [arXiv:1310.2948 [hep-th]].
- [62] J. T. Giblin and J. B. Mertens, Phys. Rev. D **90**, no. 2, 023532 (2014) [arXiv:1405.4005 [astro-ph.CO]].
- [63] J. R. Espinosa, T. Konstandin, J. M. No and G. Servant, JCAP **1006**, 028 (2010) [arXiv:1004.4187 [hep-ph]].
- [64] C. Caprini, R. Durrer and G. Servant, JCAP **0912**, 024 (2009) [arXiv:0909.0622 [astro-ph.CO]].
- [65] P. Binetruy, A. Bohe, C. Caprini and J. F. Dufaux, JCAP **1206**, 027 (2012) [arXiv:1201.0983 [gr-qc]].
- [66] A. Kosowsky, A. Mack and T. Kahniashvili, Phys. Rev. D **66**, 024030 (2002) [astro-ph/0111483].
- [67] J. M. Cornwall, R. Jackiw and E. Tomboulis, Phys. Rev. D **10**, 2428 (1974).
- [68] R. Jinno and M. Takimoto, Phys. Rev. D **95**, no. 2, 024009 (2017) [arXiv:1605.01403 [astro-ph.CO]].
- [69] S. Kuroyanagi, K. Nakayama and J. Yokoyama, PTEP **2015**, no. 1, 013E02 (2015) [arXiv:1410.6618 [astro-ph.CO]].
- [70] K. Yagi and N. Seto, Phys. Rev. D **83**, 044011 (2011) Erratum: [Phys. Rev. D **95**, no. 10, 109901 (2017)] [arXiv:1101.3940 [astro-ph.CO]].
- [71] K. Hashino, M. Kakizaki, S. Kanemura and T. Matsui, Phys. Rev. D **94**, no. 1, 015005 (2016) [arXiv:1604.02069 [hep-ph]].